2007

Preliminary Integrated Chronostratigraphy of the AND-1B Core, ANDRILL McMurdo Ice Shelf Project, Antarctica

G. S. Wilson
University of Otago, gary.wilson@stonebow.otago.ac.nz

R. H. Levy
University of Nebraska–Lincoln, rlevy2@unl.edu

G. Browne
GNS Science

R. Cody
GNS Science

N. Dunbar
New Mexico Institute of Technology

See next page for additional authors

Wilson, G. S.; Levy, R. H.; Browne, G.; Cody, R.; Dunbar, N.; Florindo, F.; Henrys, S.; Graham, I.; McIntosh, W.; McKay, R.; Naish, T. R.; Ohneiser, C.; Powell, R. D.; Ross, J.; Sagnotti, L.; Scherer, R.; Sjunneskog, C.; Strong, C. P.; Taviani, M.; Winter, D.; and ANDRILL-MIS Science Team, "Preliminary Integrated Chronostratigraphy of the AND-1B Core, ANDRILL McMurdo Ice Shelf Project, Antarctica" (2007). *ANDRILL Research and Publications*. 46.
https://digitalcommons.unl.edu/andrillrespub/46

Authors

G. S. Wilson, R. H. Levy, G. Browne, R. Cody, N. Dunbar, F. Florindo, S. Henrys, I. Graham, W. McIntosh, R. McKay, T. R. Naish, C. Ohneiser, R. D. Powell, J. Ross, L. Sagnotti, R. Scherer, C. Sjunneskog, C. P. Strong, M. Taviani, D. Winter, and ANDRILL-MIS Science Team

Preliminary Integrated Chronostratigraphy of the AND-1B Core, ANDRILL McMurdo Ice Shelf Project, Antarctica

G. Wilson[1]*, R. Levy[2], G. Browne[3], R. Cody[2,3], N. Dunbar[4], F. Florindo[5],
S. Henrys[3], I. Graham[3], W. McIntosh[4], R. McKay[6], T. Naish[3,6], C. Ohneiser[1],
R. Powell[7], J. Ross[4], L. Sagnotti[5], R. Scherer[7], C. Sjunneskog[8], C.P. Strong[3],
M. Taviani[9], D. Winter[10] & the ANDRILL-MIS Science Team[11]

[1]Department of Geology, University of Otago, PO Box 56, Dunedin - New Zealand
[2]ANDRILL Science Management Office, 126 Bessey Hall, University of Nebraska–Lincoln,
Lincoln, NE 68588-0341 - USA
[3]GNS Science, PO Box 30368, Lower Hutt - New Zealand
[4]Earth and Environmental Science Department, New Mexico Institute of Technology, 801 Leroy Place,
Socorro, NM 87801 - USA
[5]Istituto Nazionale di Geofisica e Vulcanologia, Via di Vigna Murata 605 I-00143 Rome - Italy
[6]Antarctic Research Centre, Victoria University of Wellington, PO Box 600, Wellington - New Zealand
[7]Department of Geology and Environmental Geosciences, 312 Davis Hall, Normal Road,
Northern Illinois University, De Kalb, IL 60115-2854 - USA
[8]Department of Geology and Geophysics, Louisiana State University, Baton Rouge, LA 70803 - USA
[9]Istituto di Geologia Marina, CNR, Via Gobetti 101, I-40129 Bologna - Italy
[10]Department of Geosciences, University of Nebraska–Lincoln, Lincoln, NE 68588-0340 - USA
[11]http://www.andrill.org/support/references/appendixc.html
Corresponding author (gary.wilson@otago.ac.nz)

Abstract - Chronostratigraphic data available for the preliminary age model for the upper 700 m for the AND-1B drill core include diatom biostratigraphy, magnetostratigraphy, $^{40}Ar/^{39}Ar$ ages on volcanic material, $^{87}Sr/^{86}Sr$ ages on calcareous fossil material, and surfaces of erosion identified from physical appearance and facies relationships recognised in the AND-1B drill core. The available age data allow a relatively well-constrained age model to be constructed for the upper 700 m of the drill core. Available diatom biostratigraphic constraints and $^{40}Ar/^{39}Ar$ ages allow a unique correlation of ~70% of the AND-1B magnetic polarity stratigraphy with the Geomagnetic Polarity Time Scale (GPTS). Unique correlation is not possible in several coarse diamictite intervals with closely spaced glacial surfaces of erosion and sparse microflora. However, the age model indicates relatively rapid (up to 1 m/k.y.) and continuous accumulation of intervening finer grained diatomaceous intervals punctuated by several half- to million-year hiatuses representing more than half of the last 7 m.y. in the AND-1B record. The mid- to late Pleistocene is represented by superimposed diamictite units separated from upper Pliocene alternating diamictites/diatomites by a ~1 m.y. hiatus co-incident with a regionally correlated seismic reflection surface. A *c.* 100 m-thick diatomite represents a significant portion of the early Pliocene record in the AND-1B drill core. Strata below ~620 m are late Miocene in age; however, biostratigraphic constraints are absent below 586 m and correlation with the GPTS is relatively unconstrained. At the time of writing, the only chronostratigraphic data available below 700 mbsf include three $^{40}Ar/^{39}Ar$ ages on volcanic clasts from near 1280 mbsf affording a maximum depositional age of 13.57 Ma for the base of the AND-1B drill core.

CHRONOSTRATIGRAPHIC DATA

DIATOM BIOSTRATIGRAPHY

The upper 586 metres (m) of the AND-1B drill core contains a varied and rich Plio-Pleistocene diatom flora, though abundances and preservation vary markedly with facies changes in the core. Diatomaceous-rich intervals contain multiple taxa, which provide direct correlation to Southern Ocean biostratigraphic frameworks (see Scherer et al. this volume). However, the occurrence datums throughout the AND-1B core tend to be truncated or interrupted by the rapidly varying facies, glacial/interglacial alternations, frequent hiatuses, and volcanic events recorded in the core and thus probably do not

represent the full age ranges of taxa observed in the open-ocean records. On-ice diatom data are therefore subdivided into 13 facies-based units in the core and the assemblage within each unit used to constrain the age by correlation to Southern Ocean biochronology (Tab. 1).

Diatom occurrences are limited above 150 metres below seafloor (mbsf), with thin intervals containing biostratigraphically useful species occurring at 58.15-58.90, 86.92-97.08, and 116.75-118.70 mbsf, respectively (see Scherer et al. this volume). The interval between 58.15 and 58.90 mbsf (Diatom Unit 1 or DU1) contains a mixed assemblage (Diatom Unit Assemblage 1, or DUA1), which indicates significant reworking. However, age-diagnostic

Tab. 1 - Preliminary chronsotratigraphic data for the AND-01B drill core.

Event	Datum	AND-1B Depth	Age	Error (-)	Error (+)	Sources
		(mbsf)	(Ma)	(Ma)	(Ma)	
GSE1	Glacial surface of erosion	41.10	<0.78			This paper
GSE2	Glacial surface of erosion	47.86	<0.78			This paper
GSE3	Glacial surface of erosion	51.10	<0.78			This paper
D1	LO R leventerae Bohaty	52.98	0.21	0.14	0.14	Cody et al. (2007). Zielinski & Gersonde (2002)
GSE4	Glacial surface of erosion	56.49	<0.78			This paper
D2	LO T elliptipora (Donahue) Fenner	58.15	0.68	0.38	1.13	Cody et al. (2007), Harwood & Maruyama (1992), Ramsey & Baldauf (1999), Ciesielski (1983), Baldauf & Barron (1991), Fenner (1991), Zielinski & Gersonde (2002)
DUA1top	A. actinochilus, A. ingens, R. leventerae, T. antarctica, T. elliptipora, T. lentiginosa, T. torokina - late form	58.15	0.14	0.01		Zielinski & Gersonde (2002)
DUA1bot	A. actinochilus, A. ingens, R. leventerae, T. antarctica, T. elliptipora, T. lentiginosa, T. torokina - late form	58.9	1.07			Zielinski & Gersonde (2002)
GSE5	Glacial surface of erosion	67.10	<0.78			This paper
GSE6	Glacial surface of erosion	70.37	<0.78			This paper
GSE7	Glacial surface of erosion	72.48	<0.78			This paper
MPR1	Magnetic polarity reversal (Normal above - Reversed below)	80.03	0.781			Ogg & Smith (2004)
GSE8	Glacial surface of erosion	82.74	0.80-0.97	0.05	0.04	This paper
MPR2	Magnetic polarity reversal (Reversed above - Normal below)	84.97	0.988			Ogg & Smith (2004)
A1	Felsic Tephra	85.50	1.014	0.004	0.004	This paper
D3	LO A. ingens Rattray	86.90	0.54	0.24	1.45	Cody et al. (2007), Ciesielski (1983), Baldauf & Barron (1991), Harwood & Maruyama (1992), Gersonde & Barcena (1998), Ramsey & Baldauf (1999), Winter & Iwai (2002), Zielinski & Gersonde (2002)
DUA2top	A. actinochilus, A. ingens, R. leventerae, T. antarctica, T. elliptipora, T. lentiginosa, T. torokina	86.92	0.73	0.3		Zielinski & Gersonde (2002)
D4	FO R. leventerae Bohaty	89.2 (255.70)	2.04	0.04	0.04	Cody et al. (2007)
MPR3	Magnetic polarity reversal (Normal above - Reversed below)	91.13	1.072			Ogg & Smith (2004)
S1	foraminifera	91.60	1.52	0.05	0.05	This paper
GSE9	Glacial surface of erosion	93.00	1.1-<1.65			This paper
DUA2bot	A. actinochilus, A. ingens, R. leventerae, T. antarctica, T. elliptipora, T. lentiginosa, T. torokina	97.08	1.07			Zielinski & Gersonde (2002)
GSE10	Glacial surface of erosion	99.20	>1.1-<1.65			This paper
GSE11	Glacial surface of erosion	103.73	>1.1-<1.65			This paper
GSE12	Glacial surface of erosion	109.42	>1.1-1.65			This paper
D5	LO T. vulnifica (Gombos) Fenner	(58.88) 110.39	2.17	1.57	0.93	Cody et al. (2007), Weaver & Gombos (1991), Baldauf & Barron (1991), Harwood & Maruyama (1992), Winter (1995), Gersonde & Barcena (1998), Ramsey & Baldauf (1999), Winter & Iwai (2002), Zielinski & Gersonde (2002)
A2	Basaltic Tephra	112.51	1.65	0.03	0.03	This paper
DUA3top	A. actinochilus, A. ingens, R. leventerae, T. antarctica, T. elliptipora, T. fasciculata, T. lentiginosa, T. torokina	116.75	0.84	0.09		Cody et al. (2007), Zielinski & Gersonde (2002)
DUA3bot	A. actinochilus, A. ingens, R. leventerae, T. antarctica, T. elliptipora, T. fasciculata, T. lentiginosa, T. torokina	118.7	2.08			Cody et al. (2007), Zielinski & Gersonde (2002)
GSE13	Glacial surface of erosion	124.22	1.66			This paper
D6	LO T. fasciculata Harwood & Maruyama	(58.49) 125.6	0.89	0.14	0.92	Cody et al. (2007), Harwood & Maruyama (1992), Gersonde & Burckle (1990), Zielinski & Gersonde (2002)
D7	LO A. karstenii Van Heurck	(86.90) 126.39	2.15	0.34	0.76	Cody et al. (2007), Harwood & Maruyama (1992), Zielinski & Gersonde (2002)
A3	Basaltic Tephra	136.21	1.67	0.03	0.03	This paper
GSE14	Glacial surface of erosion	150.23	1.75-<2.45			This paper
D8	LO T. inura Gersonde	(52.98) 150.7	2.54	0.66	0.56	Cody et al. (2007), Harwood & Maruyama (1992), Winter (1995), Winter & Harwood (1997), Ramsey & Baldauf (1999), Zielinski & Gersonde (2002)

Tab. 1 - Continued.

Event	Datum	AND-1B Depth	Age	Error (-)	Error (+)	Sources
D9	LO T. kolbei (Jouse) Gersonde	(86.96) 150.7	1.98	0.37	0.72	Cody et al. (2007), McCollum (1975), Ciesielski (1983), Gersonde & Burckle (1990), Baldauf & Barron (1991), Fenner (1991), Harwood & Maruyama (1992), Barron (1992), Winter (1995), Winter & Harwood (1997), Gersonde & Barcena (1998), Ramsey & Baldauf (1999), Zielinski & Gersonde (2002)
GSE15	Glacial surface of erosion	150.73	>1.75-2.45		0.1	This paper
D10	LO T. tetraoestrupii var. reimeri Mahood & Barron	150.80	1.33	0.01	0.28	Cody et al. (2007), Mahood & Barron (1996), Zielinski & Gersonde (2002)
DUA4top	A. actinochilus (rare), R. diploneides, T. elliptipora, T. inura. T. kolbei., T. oestrupii/tetraoestrupii, T. tetraoestrupii var. reimerii, T. torokina	150.87	1.46	0.15		Zielinski & Gersonde (2002)
D11	LO R. diploneides Schrader	151.21	2.62	0.11	0.07	Cody et al. (2007), Harwood & Maruyama (1992)
D12	FO A. actinochilus (Ehrenberg) Simonsen	153.80	2.77	0.57	0.42	Cody et al. (2007), Gersonde & Burckle (1990), Baldauf & Barron (1991), Harwood & Maruyama (1992), Ramsey & Baldauf (1999)
D13	FO T. tetraoestrupii var. reimeri Mahood & Barron	159.25 (190.65)	2.36	0.01	0.3	Cody et al. (2007), Mahood & Barron (1996), Zielinski & Gersonde (2002)
DUA4bot	A. actinochilus (rare). R. diploneides. T. elliptipora. T. inura. T. kolbei. T. oestrupii/ tetraoestrupii . T. tetraoestrupii var. reimerii. T. torokina	159.33	2.55			Zielinski & Gersonde (2002)
GSE16	Glacial surface of erosion	163.65	<2.58	0.2		This paper
DUA5top	A. fasciculatus, A. maccollumii, R. diploneides, T. elliptipora, T. fasciculata, T. inura, T. kolbei, T. oestrupii/tetraoestrupii, T. oliverana, T. torokina, T. vulnifica	164.1	2.25			Cody et al. (2007), Zielinski & Gersonde (2002)
D14	LO A. fasciculatus Harwood & Maruyama	164.40	2.16	0.35	0.65	Cody et al. (2007), Harwood & Maruyama (1992)
D15	LO A. maccollumii Harwood & Maruyama	177.00	2.43	0.62	0.48	Cody et al. (2007), Harwood & Maruyama (1992), Zielinski & Gersonde (2002)
DUA5bot	A. fasciculatus, A. maccollumii, R. diploneides, T. elliptipora, T. fasciculata, T. inura, T. kolbei, T. oestrupii/tetraoestrupii, T. oliverana, T. torokina, T. vulnifica	180.73	2.9		0.4	Cody et al. (2007), Zielinski & Gersonde (2002)
GSE17	Glacial surface of erosion	182.99	<2.58	0.2		This paper
DUA6top	A. maccollumii, R. diploneides, T. elliptipora (rare), T. fasciculata, T. inura, T. kolbei, T. oestrupii/ tetraoestrupii, T. oliverana, T. torokina, T. vulnifica	183.42	2.54	0.82		Zielinski & Gersonde (2002), Whitehead & Bohaty (2003)
D16	FO A. fasciculatus Harwood & Maruyama	185.05	2.71	0.99	0.06	Cody et al. (2007), Harwood & Maruyama (1992)
GSE18	Glacial surface of erosion	190.63	<2.58	0.2		This paper
MPR4	Magnetic polarity reversal (Reversed above - Normal below)	191.75	2.581			Ogg & Smith (2004)
D17	FO A. maccollumii Harwood & Maruyama	201.40	2.82	0.32	0.48	Cody et al. (2007), Harwood & Maruyama (1992), Zielinski & Gersonde (2002)
D18	FO T. vulnifica (Gombos) Fenner	201.4 (256.9)	3.15	0.95	0.36	Cody et al. (2007), Ciesielski (1983), Baldauf & Barron (1991), Harwood & Maruyama (1992), Winter (1995), Ramsey & Baldauf (1999), Winter & Iwai (2002), Whitehead & Bohaty (2004)
DUA6bot	A. maccollumii, R. diploneides, T. elliptipora (rare), T. fasciculata. T. inura, T. kolbei, T. oestrupii/ tetraoestrupii, T. oliverana, T. torokina, T. vulnifica	201.59	3.12			Zielinski & Gersonde (2002), Whitehead & Bohaty (2003)
D19	FO T. elliptipora (Donahue) Fenner	207.4 (286.6)	2.03	0.96	1.48	Cody et al. (2007), Baldauf & Barron (1991), Fenner (1991), Harwood & Maruyama (1992), Mahood & Barron (1996), Ramsey & Baldauf (1999)
DUA7top	T. fasciculata, T. elliptipora (rare), T. inura, T. oestrupii/tetraoestrupii, T. torokina	209.96	2.37	0.75		Zielinski & Gersonde (2002), Harwood & Maruyama (1992)

Tab. 1 - Continued.

Event	Datum	AND-1B Depth	Age	Error (-)	Error (+)	Sources
GSE19	Glacial surface of erosion	210.56	>2.58-<3.03			This paper
DUA7bot	T. fasciculata, T. elliptipora (rare), T. inura, T. oestrupii/tetraoestrupii, T. torokina	224.44	4.2		0.29	Zielinski & Gersonde (2002), Harwood & Maruyama (1992)
GSE20	Glacial surface of erosion	233.48	>2.58-<3.03			This paper
MPR5	Magnetic polarity reversal (Normal above - Reversed below)	248.00	3.032			This paper
DUA8top	T. fasciculata. T. inura. T. oestrupii/tetraoestrupii. T. torokina	250.02	2.37	0.75		Zielinski & Gersonde (2002), Harwood & Maruyama (1992)
GSE21	Glacial surface of erosion	251.74	>2.58-<3.21			This paper
DUA8bot	T. fasciculata. T. inura. T. oestrupii/tetraoestrupii. T. torokina	258.32	4.2		0.29	Zielinski & Gersonde (2002), Harwood & Maruyama (1992)
GSE22	Glacial surface of erosion	267.28	>2.58-<3.21			This paper
GSE23	Glacial surface of erosion	272.20	>2.58-<3.21			This paper
GSE24	Glacial surface of erosion	278.71	>2.58-<3.21			This paper
GSE25	Glacial surface of erosion	282.23	>2.58-3.21		0.1	This paper
DUA9top	F. barronii, F. praeinterfrigidaria, F. weaveri, R. diploneides, T. fasciculata, T. inura, T. oestrupii/tetraoestrupii, T. oliverana, T. striata, T. torokina	283.35	2.6	0.79		Harwood & Maruyama (1992)
D20	LO F. barronii (Gersonde) Gersonde et Barcena	(156.35) 285.36	1.24	0.44	1.36	Cody et al. (2007), Harwood & Maruyama (1992), Whitehead & Bohaty (2004), Gersonde & Burkle (1990), Ramsey & Baldauf (1999), Zielinski & Gersonde (2002)
D21	LO T. striata Harwood & Maruyama	(209.96) 285.36	2.93	1.12	0.58	Cody et al. (2007), Harwood & Maruyama (1992), Winter (1995), Winter & Harwood (1997), Zielinski & Gersonde (2002)
D22	LO F. praeinterfrigidaria (McCollum) Gersonde et Barcena	(259.83) 287.05	3.47	1.38	1.14	Cody et al. (2007), Ciesielski (1983), Harwood & Maruyama (1992), Ramsey & Baldauf (1999), Zielinski & Gersonde (2002)
D23	LO F. weaveri (Ciesielski) Gersonde et Barcena	288.33	2.49	0.66	1.24	Cody et al. (2007), Ciesielski (1983), Baldauf & Barron (1991), Fenner (1991), Harwood & Maruyama (1992), Ramsey & Baldauf (1999), Zielinski & Gersonde (2002)
D24	LO T. complicata Gersonde	(245.46) 288.8	3.4	0.79	1.11	Cody et al. (2007), Gersonde & Burckle (1990), Harwood & Maruyama (1992), Ramsey & Baldauf (1999), Zielinski & Gersonde (2002)
D25	FO F. weaveri (Ciesielski) Gersonde et Barcena	291.22	3.53	0.43	0.78	Cody et al. (2007), Baldauf & Barron (1991), Harwood & Maruyama (1992), Ramsey & Baldauf (1999), Zielinski & Gersonde (2002), Whitehead & Bohaty (2004)
DUA9bot	F. barronii, F. praeinterfrigidaria, F. weaveri, R. diploneides, T. fasciculata, T. inura, T. oestrupii/tetraoestrupii, T. oliverana, T. striata, T. torokina	292.66	3.42		0.89	Harwood & Maruyama (1992)
DUA10top	F. barronii, F. praeinterfrigidaria, R. diploneides, T. complicata, T. fasciculata, T. inura, T. oestrupii/tetraoestrupii, T. striata, T. torokina	295.46	3.12	0.51		Zielinski & Gersonde (2002), Whitehead & Bohaty (2003)
D26	FO F. barronii (McCollum) Gersonde et Barcena	345.95	4.4	0.39	0.4	Cody et al. (2007), Gersonde & Burckle (1990), Baldauf & Barron (1991), Harwood & Maruyama (1992), Ramsey & Baldauf (1999), Winter & Iwai (2002), Whitehead & Bohaty (2004)
MPR6	Magnetic polarity reversal (Reversed above - Normal below)	346.00	3.33		0.857	This paper
GSE26	Glacial surface of erosion	346.03	>3.2-<4.19			This paper
DUA10bot	F. barronii, F. praeinterfrigidaria, R. diploneides, T. complicata, T. fasciculata, T. inura, T. oestrupii/tetraoestrupii, T. striata, T. torokina	346.94	4.16		0.55	Zielinski & Gersonde (2002), Whitehead & Bohaty (2003)
GSE27	Glacial surface of erosion	346.94	>3.2-<4.19	0.15	1.1	This paper
DUA11top	F. praeinterfrigidaria, R. diploneides, T. complicata, T. fasciculata, T. inura, T. oestrupii/tetraoestrupii, T. striata, T. torokina	363.37	4.16	0.15		Zielinski & Gersonde (2002), Whitehead & Bohaty (2003), absence of F. baronii
GSE28	Glacial surface of erosion	364.18	>3.2-<4.19			This paper

Tab. 1 - Continued.

Event	Datum	AND-1B Depth	Age	Error (-)	Error (+)	Sources
D27	LO F. interfrigidaria (McCollum) Gersonde et Barcena	364.38	2.43	0.62	0.87	Cody et al, (2007), Weaver & Gombos (1991), Baldauf & Barron (1991), Harwood & Maruyama (1992), Ramsey & Baldauf (1999), Zielinski & Gersonde (2002)
GSE29	Glacial surface of erosion	372.38	>3.2-<4.19			This paper
GSE30	Glacial surface of erosion	375.85	>3.2-4.19			This paper
D28	FO T. fasciculata Harwood & Maruyama	429.9 (450.83)	4.34	0.09	0.15	Cody et al. (2007), Harwood & Maruyama (1992)
D29	FO T. kolbei (Jouse) Gersonde	435.02	3.91	1.68	0.88	Cody et al. (2007), Baldauf & Barron (1991), Fenner (1991), Harwood & Maruyama (1992), Ramsey & Baldauf (1999)
D30	FO F. praeinterfrigidaria (McCollum) Gersonde et Barcena	437.59	4.75	0.24	1.05	Cody et al. (2007), Gersonde & Burkle (1990), Baldauf & Barron (1991), Harwood & Maruyama (1992), Ramsey & Baldauf (1999), Censarek & Gersonde (2002)
MPR7	Magnetic polarity reversal (Normal above - Reversed below)	440.00	4.3			This paper
D31	FO T. striata Harwood & Maruyama	452.25	4.47	0.17	0.17	Cody et al. (2007), Harwood & Maruyama (1992)
MPR8	Magnetic polarity reversal (Reversed above - Normal below)	453.00	4.493			This paper
DUA11bot	F. praeinterfrigidaria, R. diploneides, T. complicata, T. fasciculata, T. inura, T. oestrupii/tetraoestrupii, T. striata, T. torokina	459.24	5.06		1.76	Zielinski & Gersonde (2002), Whitehead & Bohaty (2003)
MPR9	Magnetic polarity reversal (Normal above - Reversed below)	460.00	4.631			This paper
GSE31	Glacial surface of erosion	467.41	>4.63-<4.8			This paper
GSE32	Glacial surface of erosion	471.53	>4.63-<4.8			This paper
GSE33	Glacial surface of erosion	479.32	>4.63-<4.8			This paper
DUA12top	R. diploneides, T. oestrupii/tetraoestrupii, T. complicata, T. oliverana, T. torokina	503.42	4.5*			Shipboard Scientific Party (2001), *absence of T. striata & T. inura (Harwood & Maruyama, 1992; Zielinski & Gersonde, 2002)
D32	FO T. inura Gersonde	507 (565.67)	4.74	0.03	2.09	Cody et al. (2007), Ciesielski (1983), Gersonde & Burckle (1990), Baldauf & Barron (1991), Harwood & Maruyama (1992), Censarek & Gersnde (2002), Whitehead & Bohaty (2004)
D33	FO F. praeinterfrigidaria (McCollum) Gersonde et Barcena	508.95 (566.16)	4.75	0.24	0.95	Cody et al. (2007), Gersonde & Burkle (1990), Baldauf & Barron (1991), Harwood & Maruyama (1992), Ramsey & Baldauf (1999), Censarek & Gersonde (2002)
D34	FO R. antarctica Heiden, in Heiden & Kolbe	509.10	4.5	0.07	0.07	Cody et al. (2007)
DUA12bot	R. diploneides, T. oestrupii/tetraoestrupii, T. complicata, T. oliverana, T. torokina	511.56	5.06			Shipboard Scientific Party (2001), *absence of T. striata & T. inura (Harwood & Maruyama, 1992; Zielinski & Gersonde, 2002)
GSE34	Glacial surface of erosion	514.28	>4.63-<4.8			This paper
MPR10	Magnetic polarity reversal (Reversed above - Normal below)	520.00	4.799			This paper
GSE35	Glacial surface of erosion	537.82	>4.8-<4.9			This paper
GSE36	Glacial surface of erosion	563.31	>4.8-<4.9			This paper
DUA13top	R. diploneides, T. complicata, T. oestrupii/tetraoestrupii, T. oliverana, T. torokina, T. tumida (rare)	565.67	4.5*			Shipboard Scientific Party (2001), *absence of T. striata & T. inura (Harwood & Maruyama, 1992; Zielinski & Gersonde, 2002)
D35	FO R. diploneides Schrader	581.84	4.66	0.17	0.04	Cody et al. (2007), Harwood & Maruyama (1992)
D36	FO T. complicata Gersonde	583.64	4.68	0.17	0.12	Cody et al. (2007), Gersonde & Burkle (1990), Harwood & Maruyama (1992), Ramsey & Baldauf (1999)
D37	FO T. oestrupii (Ostenfield) Proschkina-Lavrenko	583.64	4.88	0.57	1.08	Cody et al. (2007), Baldauf & Barron (1991), Harwood & Maruyama (1992), Barron (1992), Ramsey & Baldauf (1999)
DUA13bot	R. diploneides, T. complicata, T. oestrupii/tetraoestrupii, T. oliverana, T. torokina, T. tumida (rare)	586.45	5.7		0.64	Shipboard Scientific Party (2001), *absence of T. striata & T. inura (Harwood & Maruyama, 1992; Zielinski & Gersonde, 2002)
MPR11	Magnetic polarity reversal (Normal above - Reversed below)	596.00	4.896			This paper
GSE37	Glacial surface of erosion	615.50	>4.9-<6.2			This paper
GSE38	Glacial surface of erosion	622.00	>4.9-<6.2			This paper
GSE39	Glacial surface of erosion	624.00	>4.9-<6.2			This paper
MPR12	Magnetic polarity reversal (Reversed above - Normal below)	630.00	6.033	1.036		This paper
GSE40	Glacial surface of erosion	635.00	>4.9-<6.25			This paper

Tab. 1 - Continued.

Event	Datum	AND-1B Depth	Age	Error (-)	Error (+)	Sources
MPR13	Magnetic polarity reversal (Normal above - Reversed below)	638.00	6.252			This paper
A4	Groundmass concentrate of basaltic lava flow	648.37	6.48	0.13	0.13	This paper
MPR14	Magnetic polarity reversal (Reversed above - Normal below)	655.00	6.436			This paper
GSE41	Glacial surface of erosion	674.00	>6.44			This paper
A5	Sanadine from volcanic clast	1277.91	<13.82	0.09	0.09	This paper
A6	Sanadine from volcanic clast	1278.84	<13.85	0.18	0.18	This paper
A7	Sanadine from volcanic clast	1279.00	<13.57	0.13	0.13	This paper

species include *Actinocyclus actinochilus, Thalassiosira gracilis, T. antarctica, T. elliptipora, A. ingens,* and *Rouxia leventerae*. A conservative age range of 0.14–1.07 Ma is indicated by the co-occurrence of *R. leventerae* and *T. antarctica* (Zielinski & Gersonde 2002). Diatom preservation and abundance is better between 86.92 and 97.08 mbsf (DUA2), although many reworked forms are still present (see Scherer et al. this volume). The assemblage is dominated by fragments of *Thalassionema* and *Thalassiothrix* and abundant *Chaetoceros* spp. Age-definitive forms are similar to the 58.15–58.90 mbsf interval; however. *T. elliptipora* is more abundant, allowing a tighter age constraint for this interval of 0.73–1.07 Ma (Zielinski & Gersonde 2002). The assemblage between 116.75 and 118.70 bsf (DUA3) includes more abundant *A. ingens*, which has a last common occurrence around Antarctica reported at 0.67 Ma. and *T. fasciculata* with a last occurrence (LO) of 0.84 Ma (Zielinski & Gersonde 2002). The late form of *T. torokina* is also present and the assemblage compares closely with that described from lithostratigraphic subunit 3.2 in Cape Roberts Project (CRP)-1 and dated at 0.75–1.15 Ma (Bohaty et al. 1998). A conservative age of 0.84–2.08 Ma is adopted for DUA3.

Multiple diatomaceous and diatomite intervals occur between 150 and 586 mbsf, with high abundances, good preservation and minimal reworking (see Scherer et al. this volume). Between 150.87 and 159.33 mbsf (DU4), the assemblage (DUA4) is dominated by abundant *Rouxia antarctica* and a diverse *Fragilariopsis* flora. Age-diagnostic species include *T. kolbei, R. diploneides, T. inura*, and *T. tetraoestrupii* var. *reimerii*. Occurrence of the latter is restricted to this interval of the AND-1B core. T. *tetraoestrupii* var. *reimerii* ranges between 1.46 and 2.55 Ma (Zielinski & Gersonde 2002), defining the possible age of DUA4. Between 164.1 and 180.73 bsf (DU5). *A. fasciculatus* and *A. maccollumii* constrain the age to between 2.25 and 2.9 Ma (DUA5) (Zielinski & Gersonde 2002; Cody et al. in press). This interval also likely contains the LO of *T. vulnifica,* although potentially reworked forms are seen higher in the core. which has an age of 2.41 Ma (Zielinski & Gersonde 2002). Two thin diatomaceous layers with similar flora span a diamictite unit between 183.42 and 201.59 mbsf (DUA6). Age-diagnostic species include *A. maccollumii* and *A. fasciulatus.* which last occur between the two diatomaceous layers, and *T.vulnifica*, which first occurs at the base of the lower of the two

diatomaceous layers (180.73 mbsf). A conservative age range between <2.58 and 3.12 Ma is indicated for DUA6 by the top of the *A. maccollumii* range (Zielinski & Gersonde 2002) and the first occurrence (FO) of *T. vulnifica* (Whitehead & Bohaty 2003), respectively.

Two diatomaceous units between 209.96 and 224.44 mbsf (DU7) and 250.02 and 258.32 mbsf (DUA8) contain a wide-ranging flora (see Scherer et al. this volume) and the best age constraint is afforded by *T. inura* and *T. fasciculata,* which occur in moderately high abundance and suggest an age range of between 2.37 and 4.2 Ma for DUA7 and DUA8 (Harwood & Maruyama 1992; Zielinski & Gersonde 2002). Lower in the core, 283.35–292.66 mbsf (DUA9), *Fragilariopsis praeinterfrigidaria, F. barronii,* and *T. striata* are more consistently observed, but better constraint is afforded by *Fragilariopsis weaverii*, the occurrence of which is restricted to this interval and provides an age constraint for DUA9 of between 2.6 and 3.42 Ma (Harwood & Maruyama 1992). The diamictite between 295.46 and 346.94 mbsf (DUA10) is relatively diatom rich with moderate to poor preservation of individual forms. *F. praeinterfrigidaria* and *F. barronii* are both present and indicate an *in situ* flora as they are both relatively small and fragile. An age range between 3.12 and 4.16 Ma is indicated for DUA10 by the concurrent range of *T. complicata* and *F. barronii* (Zielinski & Gersonde 2002; Whitehead & Bohaty 2003).

The interval between 377 and 459 mbsf in the core is described as diatomite (see Krissek et al. this volume) and is coincident with a single diatom assemblage (DUA11), which occurs between 363.37 and 459.24 mbsf. Age-diagnostic forms include *F. praeinterfrigidaria, R. diploneides, T. complicata, T. fasciculata, T. inura, T. oestrupii/tetraoestrupii, T. striata,* and *T. torokina*. The presence of *Thalassiosira inura* restricts this unit to between 2.37 and 5.06 Ma in age (Whitehead & Bohaty 2003; Zielinski & Gersonde 2002). However, the absence of *F. barronii* in such a rich assemblage suggests an age range between 4.16 and 5.06 Ma. Two further diatom-rich units are encountered below 500 mbsf in the core. One between 503.42 and 511.56 mbsf (DU12) and the other between 565.67 and 586.45 mbsf (DU13). The two units contain a similar diatom flora and again the age is constrained as much by the absence as by the presence of species. *Thalasssiosira fasciculata,T. inura,*and *T. striata*, while observed higher in the core,are not observed in this interval, thus an age older than the FO of *T. inura* (5.03 Ma) is suggested.

However, the presence of *T. complicata* and *R. diploneides* might indicate a slightly younger age, therefore a conservative upper limit of 4.5 Ma is given for these assemblages (DUA12 and DUA13). *Thalassiosira oestrupii* is also present in both units and indicates an age younger than its first occurrence (5.7 Ma; Shipboard Scientific Party. 2001).

Ages for first and last occurrence datums of key diatom taxa presented in figure 4 and table 1 were derived in a quantitative evaluation of diatom events and palaeomagnetic reversals from 32 Neogene sections in the Southern Ocean and around the Antarctic continental margin (Cody et al. 2007). Cody et al. (2007), employed Constrained Optimization (CONOP), a computer assisted multidimensional version of graphic correlation (Shaw 1964) to generate a deterministic composite model and average-range composite model. The deterministic model is based on the total or maximum ranges of diatoms and was created by constraining candidate sequences to honour observed coexistences and allowing local range ends to be extended only to fit the test sequence. The average composite model is based on the average ranges of diatoms and was created by relaxing the constraint against range contractions and allowing both local FO and LO datums to move either up- or down-section to find the most parsimonious fit to the global sequence. A range in age for a given datum reflects its minimum and maximum best-fit position in the composite sequence.

We utilised the average composite range model of Cody et al. (2007) to help develop the initial age model for the upper 700 m of the AND-1B drill core. The average range model, which imitates the modal solution aimed for by probabilistic methods, is likely more pertinent to the preliminary analysis of new drill cores. Its sequence of events represents the most likely order in which they will be observed in the next section studied (Cooper et al. 2001). Error values listed in table 1 were determined by calculating the difference between the CONOP model age and the maximum and minimum age for each datum identified through a search of published articles.

$^{40}Ar/^{39}Ar$ AGES

Preliminary $^{40}Ar/^{39}Ar$ dating of 13 volcanic samples from four stratigraphic intervals within the AND-1B core provides key age-stratigraphic constraints for the development of an accurate age model. To date, seven analyses have yielded statistically robust and stratigraphically meaningful ages (Tab. 2). The four different stratigraphic intervals represented by the seven successfully dated samples are: (1) 85.53–85.85 mbsf felsic tephra, (2) ~112–145 mbsf basaltic tephra, (3) 646.30–649.34 mbsf basaltic lava flow, and (4) ~1280 mbsf volcanic clasts. Analysis of most of the suitable material collected during core sampling in McMurdo has been completed. In the future, we hope to refine the ages of the already dated intervals and identify new dating targets.

All samples were prepared at the New Mexico Geochronology Research Laboratory (NMGRL) in Socorro, NM, with the exception of sample 85.53–85.85 mbsf, which was prepared at McMurdo Station. Sample preparation was tailored to each sample in order to optimise results. Sample 85.53–85.85 mbsf underwent ultrasonic cleaning, in order to remove any adhering volcanic glass or clay minerals, followed by hand picking of K-feldspar grains at McMurdo Station. Four basaltic tephra samples (112.51–112.62 mbsf, 136.21–136.27 mbsf, 140.30–140.36 mbsf, and 145.12–145.16 mbsf) were purified by extensive rinsing, sieving, acid treatment, magnetic separation and ultrasonic cleaning in an attempt to remove contaminants and hydration rims observed during electron microprobe sample characterisation. The 648.37–648.43 mbsf lava sample was mechanically crushed and hand sieved. The 300–500 μm sieve fraction, used for $^{40}Ar/^{39}Ar$ analysis, was treated with 10% HCl for 10 minutes followed by ultrasonic cleaning in distilled water in order to separate and remove any alteration phases from the primary volcanic material. K-feldspar phenocrysts, ranging in size from 355 to 500 μm, from the three volcanic clasts (1277.91-1277.95 mbsf, 1278.84-1278.87 mbsf, and 1279.00–1 79.04 mbsf) were easily removed by crushing and magnetic separation followed by hand picking to remove any contaminant grains. See table 2 for more sample preparation information. Samples were packaged with flux monitors of known age (Fish Canyon Tuff sanidine, 28.02 Ma; Renne et al. 1998) and irradiated for 7 hours at the reactor facility at Texas A&M, College Station, TX, except for the 85.53–85.85 mbsf K-feldspar separate sample, which was only irradiated for 1 hour. $^{40}Ar/^{39}Ar$ analyses were preformed using either the CO_2 laser or resistance furnace systems at NMGRL. Further information on the instrumentation used at NMGRL, as well as details of analytical procedures, are located in the notes section of table 2.

85.53–85.85 mbsf Felsic Tephra (1.014 ± 0.004 Ma). Euhedral sanidine phenocrysts separated from the 85.53–85.85 mbsf pumice-rich layer were used for $^{40}Ar/^{39}Ar$ analysis. Following irradiation of the sample grains ranging in size from 200 to 600 μm, single crystals and groups of two to three crystals were fused by a CO_2 laser, and then analysed by the MAP-215-50 mass spectrometer. Compiled data from 37 sanidine phenocrysts from the 85.53–85.85 mbsf tephra (Tab. 3) yielded a precise, robust isochron age of 1.014 ± 0.004 Ma. The data form a unimodal normal distribution after rejecting two older crystals interpreted as xenocrysts (Fig. 1A). On an isochron diagram (Fig.1B) the data form a well-aligned linear array indicating small but significant amounts of excess ^{40}Ar. The isochron age is interpreted as an accurate determination of the eruption age of the 85.53–85.85 mbsf tephra.

~112–145 mbsf Basaltic Tephra (1.65 ±0.03 to 1.67 ±0.03 Ma). Two purified glass samples from the 112–145 mbsf basaltic tephra interval yielded

Tab. 2 - Summary of $^{40}Ar/^{39}Ar$ results.

									Preferred Age					
Sample	*Location (mbsf)*	*L#*	*Irrad*	*Material*	*analysis*	*n*	*MSWD*	*K/Ca*	*±*	*2σ*	*Age (Ma)*	*±*	*2σ*	
AN85-1	85.53-85.87	56529	NM-198M	K-spar	Isochron	37	1.2	19.5	±	18.3	1.014	±	0.004	
An112_51	112.51-112.62	56873-01	NM-203P	Glass	Isochron	9	2	0.2	±	0.0	1.65	±	0.05	
An136_21	136.21-136.27	56867-01	NM-203O	Glass	Isochron	11	1	0.3	±	0.1	1.67	±	0.05	
648-GM-HCl	648.37-648.43	56788-01	NM-203C	WR	Plateau	6	1.7	0.4	±	0.3	6.48	±	0.13	
1277-91	1277.91-1277.95	56793	NM-203D	K-spar	Mean	15	0.3	31.0	±	30.4	13.82	±	0.09	
1278-84	1278.84-1278.97	56794	NM-203D	K-spar	Mean	14	0.5	1854.7	±	11014.7	13.85	±	0.18	
1279-00	1279.00-1279.04	56792	NM-203D	K-spar	Mean	15	0.5	8.7	±	5.8	13.57	±	0.13	

L# = Lab number. Irrad = Irradiation number and tray letter. n = number of analyses use to compute age. MSWD = Mean Square Weighted Deviation

Notes

Sample preparation and irradiation:
- Samples were mechanically crushed and hand sieved at NMGRL
- Sieve fractions 106-125 μm were used for sample An112_51 and 136_21, and 300-500 μm for 648-GM-HCl
- K-feldspar phenocrysts from samples AN85-1, 1277-91, 1278-84, 1279-00 were hand picked under a stereo microscope
- Samples treated with acid were immersed in 10% HCl within an ultrasonic bath. followed by ultrasonic rinsing with distilled water to remove the residual acid.
- All samples and neutron flux monitors were loaded into machine Al discs in a known geometry
- Neutron flux monitor Fish Canyon Tuff sanidine (FC-1). Assigned age = 28.02 Ma (Renne et al. 1998)

Instrumentation:
- Mass Analyzer Products 215-50 mass spectrometer on line with automated all-metal extraction system.
- Separate was step-heated using a Mo double-vacuum resistance furnace. Heating duration in the furnace was 10 minutes
- Reactive gases removed during furnace analysis by reaction with 3 SAES GP-50 getters. 2 operated at ~450°C and 1 at 20°C. Gas also exposed to a W filament operated at ~2000°C.

Analytical parameters:
- Averaged furnace sensitivity 1.24×10^{-16} moles/pA. Averaged laser sensitivity 7.12×10^{-17} moles/pA.
- Total system blank and background for the furnace averaged 5017, 5.6, 6.5, 29.1, 7.8, 21.7×10^{-18} moles.
- Total system blank and background for the laser averaged 376, 5.3, 1.9, 5.6, 7.8, 29.7×10^{-18} moles.
- J-factors determined to a precision of ± 0.1% by CO_2 laser-fusion of 4 to 6 single crystals from each of the 6 or 10 radial positions
- around the irradiation tray (6 for a 12 hole disc. 10 for a 20 hole disc).
- Correction factors for interfering nuclear reactions were determined using K-glass and CaF2 and are as follows: $(^{40}Ar/^{39}Ar)_K = 0 \pm 0.0004$; $(^{36}Ar/^{37}Ar)_{Ca} = 0.000289 \pm 0.000005$; and $(^{39}Ar/^{37}Ar)_{Ca} = 0.00068 \pm 0.00002$

Age calculations:
- Plateau age or preferred age calculated for the indicated steps by weighting each step by the inverse of the variance.
- Plateau age error is inverse-variance-weighted mean error (Taylor, 1982) times root MSWD where MSWD>1.
- MSWD values are calculated for n-1 degrees of freedom for plateau age.
- Isochron ages. $^{40}Ar/^{36}Ar_i$ and MSWD values calculated from regression results obtained by the methods of York (1969).
- Decay constants and isotopic abundances after Steiger and Jäger (1977).
- All errors reported at ±2σ. unless otherwise noted.

precise ages that are concordant within uncertainty. As described in the on-ice report of preliminary results one non-purified glass sample (114.47–114.51 mbsf) yielded a discordant spectrum, suggesting an age of approximately 2 Ma. The four purified glass samples were incrementally heated in a resistance furnace. Two samples yielded precise isochron ages 112.51–112.62 mbsf, 1.65 ±0.03 Ma, Fig. 1D; 136.21–136.27 mbsf, 1.67 ±0.03 Ma. Fig. 1F; Tab. 4) while the other two (140.30–140.36 mbsf and 145.12–145.16 mbsf) yielded spectra indicative of contamination by older material. Further sample purification work needs to be done to better date the bottom of this basaltic tephra section, thereby constraining the duration of the eruptive interval.

646.30–649.34 mbsf Basaltic Lava Flow (6.48 ±0.13 Ma). A whole-rock sample (648.37–648.43 mbsf) from the basaltic lava flow located near the middle of the core was incrementally heated in the resistance furnace, yielding a moderately robust plateau age of 6.48 ± 0.13 Ma (Fig. 1G; Tab. 5). This lava flow was identified in McMurdo as an attractive dating target. Electron microprobe sample characterisation indicates that the lava consists of a glassy groundmass containing abundant calcic plagioclase phenocrysts with K-bearing rims. The isochron plot for this sample yielded an isochron age within 2σ uncertainty of the plateau age. In addition, the isochron produced an initial $^{40}Ar/^{36}Ar$ value within 2σ uncertainty of the atmospheric value ($[^{40}Ar/^{36}Ar]_{atm}$ = 295.5). The age spectrum results for this sample, in conjunction with the results of an isochron plot, yield what we believe to be an accurate eruption age of 6.48 ± 0.13 Ma.
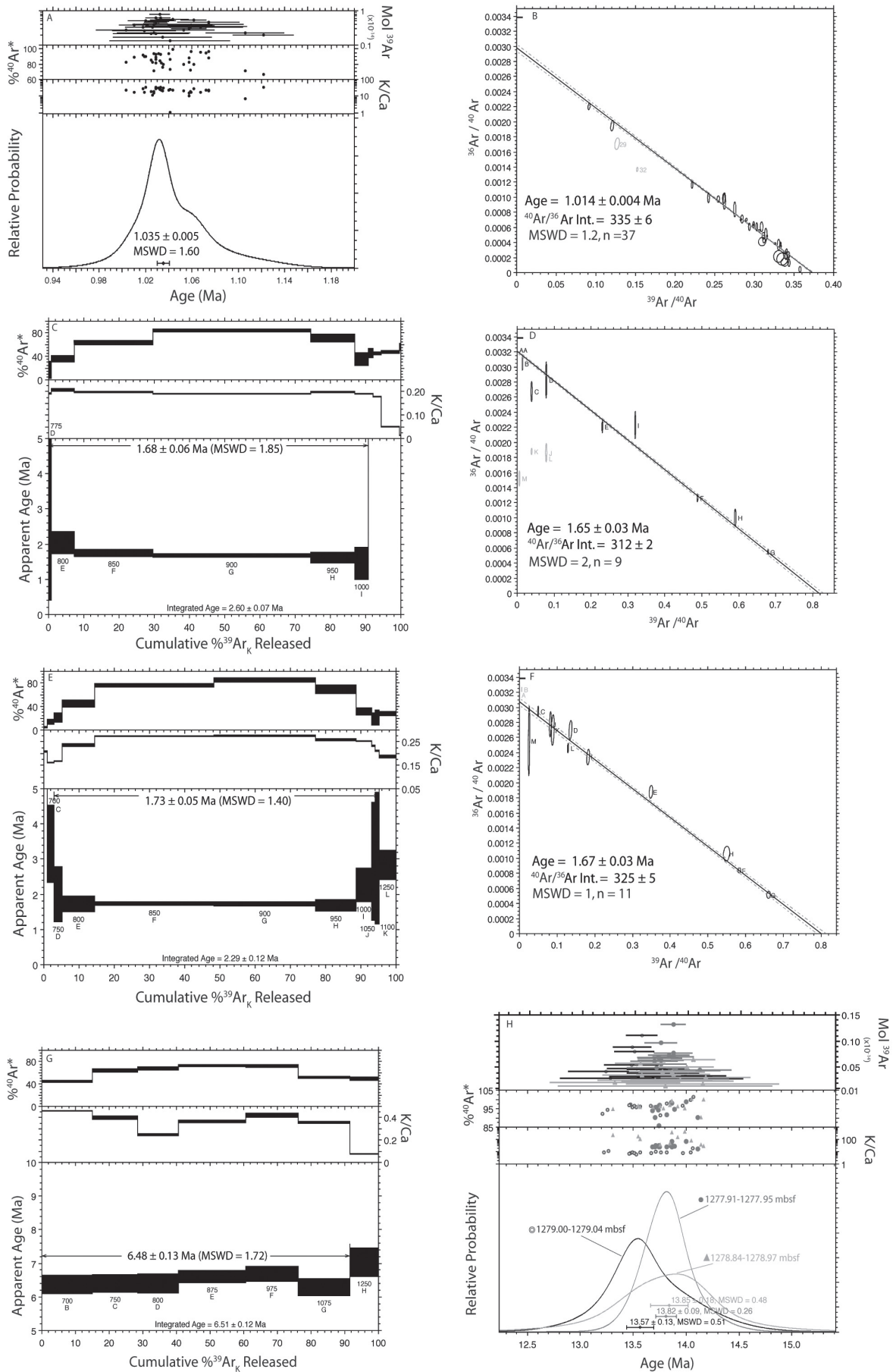
Fig. 1 – (A) Age probability plot and (B) 'inverse' isochron for 85.35– 85.85 mbsf K-feldspars; (C) age spectrum and (D) 'inverse' isochron for 112.51–112.62 mbsf glass; (E) age spectrum and (F) 'inverse' isochron for 136.21–136.27 mbsf glass; (G) age spectrum for 648.37–648.43 mbsf whole rock, and (H) age probability plot for ~1 280 mbsf volcanic clasts.

Tab. 3 - ^{40}Ar/^{39}Ar analytical data for 85.53–85.83 mbsf pumice-rich layer.

ID	^{40}Ar/^{39}Ar	^{37}Ar/^{39}Ar	^{36}Ar/^{39}Ar	^{39}Ar$_K$	K/Ca	40Ar*	Age	±1σ
			(x 10^{-3})	(x 10^{-15} mol)		(%)	(Ma)	(Ma)
AN85-1. Sanidine. J=0.0002096±0.09%. D=1.002±0.001. NM-198M. Lab#=56528 and 56529								
35	3.229	0.023	1.962	4.254	22.5	82.1	1.004	0.024
12	3.006	0.032	1.133	5.851	16.0	89.0	1.011	0.011
13	2.938	0.019	0.833	4.974	26.4	91.7	1.018	0.011
25	3.019	0.031	1.113	4.015	16.4	89.2	1.019	0.025
24	2.999	0.015	1.030	7.815	33.9	89.9	1.021	0.013
40	3.176	0.030	1.595	3.208	17.2	85.2	1.025	0.031
42	3.298	0.046	2.000	5.102	11.1	82.2	1.026	0.021
36	3.816	0.036	3.741	3.491	14.2	71.1	1.027	0.030
23	2.910	0.030	0.667	6.207	17.1	93.3	1.028	0.016
10	3.167	0.019	1.509	7.091	27.0	86.0	1.029	0.008
06	2.948	0.018	0.767	6.506	28.0	92.4	1.029	0.009
09	3.343	0.016	2.102	3.209	31.5	81.5	1.029	0.018
01	3.065	0.016	1.162	9.430	31.3	88.8	1.029	0.007
02	2.916	0.018	0.641	7.396	28.6	93.6	1.031	0.008
03	3.267	0.020	1.817	11.977	25.1	83.6	1.033	0.007
14	2.959	0.016	0.768	9.339	32.9	92.4	1.033	0.007
11	3.354	0.024	2.103	8.304	21.7	81.5	1.034	0.008
37	3.631	0.027	3.042	2.523	19.1	75.3	1.035	0.041
04	3.448	0.018	2.404	7.685	29.1	79.4	1.035	0.001
43	2.939	0.024	0.654	5.654	21.5	93.5	1.040	0.018
38	3.808	0.501	3.721	2.042	1.0	72.2	1.041	0.050
45	3.204	0.022	1.539	5.257	23.7	85.9	1.041	0.020
21	2.791	0.024	0.123	8.594	21.4	98.8	1.044	0.012
44	3.508	0.025	2.464	4.214	20.6	79.3	1.053	0.025
07	3.199	0.052	1.374	4.525	9.8	87.4	1.058	0.013
41	3.400	0.036	2.059	5.474	14.2	82.2	1.058	0.020
22	3.916	0.027	3.792	5.050	18.7	71.4	1.059	0.022
26	2.906	0.031	0.373	5.966	16.5	96.3	1.059	0.017
05	3.533	0.019	2.456	7.975	26.4	79.5	1.062	0.009
27	2.978	0.030	0.540	5.013	16.9	94.7	1.068	0.035
30	3.021	0.024	0.645	5.275	21.4	93.8	1.072	0.034
31	2.954	0.025	0.394	7.228	20.7	96.1	1.075	0.025
28	3.223	0.024	1.304	6.088	21.3	88.1	1.075	0.029
39	4.126	0.075	4.094	3.514	6.8	70.8	1.106	0.032
08	4.515	0.015	5.241	2.981	33.7	65.7	1.122	0.025
34	8.270	0.716	16.25	2.322	0.71	42.6	1.335	0.079
33	10.88	0.048	23.96	2.946	10.6	35.0	1.440	0.062
29	7.853	0.322	13.43	1.949	1.6	49.8	1.481	0.089
32	6.559	0.218	9.005	8.475	2.3	59.7	1.482	0.025
Mean age ± 2σ	n=39	MSWD=12.03			19.5 ±18.3		1.040	0.015

Notes:
- Isotopic ratios corrected for blank, radioactive decay, and mass discrimination, not corrected for interfering reactions.
- Errors quoted for individual analyses include analytical error only, without interfering reaction or J uncertainties.
- Mean age is weighted mean age of Taylor (1982). Mean age error is weighted error of the mean (Taylor, 1982), multiplied by the root of the MSWD where MSWD>1, and also incorporates uncertainty in J factors and irradiation correction uncertainties.
- Decay constants and isotopic abundances after Steiger & Jäger (1977).
- # symbol preceding sample ID denotes analyses excluded from mean age calculations.
- Ages calculated relative to FC-2 Fish Canyon Tuff sanidine interlaboratory standard at 28.02 Ma
- Decay Constant (LambdaK (total)) = 5.543e-10/a
- Correction factors:
  - (^{39}Ar/^{37}Ar)$_{Ca}$ = 0.00068 ± 2e-05
  - (^{36}Ar/^{37}Ar)$_{Ca}$ = 0.00028 ± 1e-05
  - (^{38}Ar/^{39}Ar)$_K$ = 0.013
  - (^{40}Ar/^{39}Ar)$_K$ = 0 ± 0.0004

~1280 mbsf Volcanic Clasts (maximum depositional age 13.57 ± 0.13 Ma). After failing to find fresh K-feldspar phenocrysts in altered pumice from the bottom of the core, we dated three volcanic clasts from near 1280 m in an attempt to determine a maximum depositional age. In contrast to the altered tephra, these volcanic clasts contain large fresh sanidine crystals. Fifteen sanidine phenocrysts separated from each of these clasts were individually fused using a CO_2 laser. Sanidine from each of these three clasts yields tightly grouped normal age distributions (Tab. 6). Weighted mean ages for the three clasts are (1277.91–1277.95 mbsf, 13.82 ± 0.09 Ma; 1278.84–1278.87 mbsf, 13.85 ± 0.18 Ma; and 1279.00–1279.04 mbsf, 13.57 ± 0.13 Ma; Fig. 1H). Although these clasts do not directly date the depositional age of the bottom of the core, they do provide a precise and accurate maximum depositional age of 13.57 ± 0.13 Ma for the sediment at 1279.00 mbsf.

Tab. 4 - ^{40}Ar/^{39}Ar analytical data for 112.51–112.61 and 136.31–136.27 mbsf basaltic.

	ID	Temp (°C)	^{40}Ar/^{39}Ar	^{37}Ar/^{39}Ar	^{36}Ar/^{39}Ar (x 10^{-3})	^{39}Ar$_K$ (x 10^{-15} mol)	K/Ca	^{40}Ar* (%)	^{39}Ar (%)	Age (Ma)	±1σ (Ma)
An112_51. Glass. 53.08 mg. J=0.0007472±0.07%. D=1.002±0.001. NM-203P. Lab#=56873-01										
x	AA	500	26808.7	3.023	86308.8	0.008	0.17	4.9	0.0	1228.1	222.6
x	B	600	66.82	2.911	204.0	0.326	0.18	10.1	0.4	9.1	2.4
x	C	700	24.25	3.208	65.59	0.569	0.16	21.2	1.2	6.9	1.3
	D	750	12.44	2.668	35.87	0.594	0.19	16.6	2.0	2.8	1.2
	E	800	4.312	2.490	10.20	4.93	0.20	34.9	8.5	2.03	0.16
	F	850	2.041	2.596	3.292	16.76	0.20	62.9	30.6	1.732	0.049
	G	900	1.468	2.682	1.542	33.4	0.19	84.1	74.8	1.665	0.025
	H	950	1.686	2.592	2.410	9.31	0.20	70.5	87.1	1.605	0.077
	I	1000	3.117	2.718	7.691	2.90	0.19	34.3	90.9	1.44	0.23
xi	J	1050	12.37	2.711	23.70	1.023	0.19	45.2	92.3	7.54	0.64
xi	K	1100	24.53	2.868	46.76	1.730	0.18	44.6	94.6	14.72	0.45
xi	L	1250	12.52	10.52	25.24	3.98	0.049	47.3	99.8	8.03	0.21
xi	M	1700	123.9	40.11	199.1	0.144	0.013	55.2	100.0	92.4	5.2
	Integrated age ± 2σ		n=13			75.7	0.16	K$_2$O=0.73%		2.849	0.098
	Plateau ± 2σ	steps D-I	n=6	MSWD=1.85		67.9	0.19 ±0.01		89.7	1.678	0.057
	Isochron±2σ	steps AA-I	n=9	MSWD=1.99			^{40}Ar/^{36}Ar=311.9±3.5			1.648	0.045
An136_21. Glass. 53.3 mg. J=0.0007416±0.07%. D=1.002±0.001. NM-203O. Lab#=56867-01										
xi	A	500	27907.1	2.833	88181.1	0.014	0.18	6.6	0.0	1558.8	267.1
xi	B	600	154.0	2.468	498.9	0.954	0.21	4.4	1.0	9.1	1.7
x	C	700	19.68	3.164	58.82	1.922	0.16	13.0	3.0	3.42	0.55
	D	750	7.283	3.097	20.49	2.34	0.16	20.4	5.3	1.99	0.39
	E	800	2.857	2.187	5.955	8.87	0.23	44.7	14.4	1.71	0.11
	F	850	1.710	1.868	1.943	33.2	0.27	75.5	48.3	1.728	0.030
	G	900	1.511	1.867	1.288	28.2	0.27	85.0	77.1	1.720	0.034
	H	950	1.817	1.984	2.474	11.34	0.26	68.8	88.7	1.674	0.080
	I	1000	5.431	2.030	13.25	4.19	0.25	31.0	93.0	2.25	0.24
	J	1050	12.05	2.193	34.01	1.059	0.23	18.1	94.1	2.92	0.84
	K	1100	11.08	2.421	30.54	0.982	0.21	20.4	95.1	3.02	0.94
x	L	1250	7.699	2.737	19.66	4.68	0.19	27.5	99.9	2.83	0.21
x	M	1700	38.21	16.49	102.0	0.119	0.031	24.7	100.0	12.7	7.4
	Integrated age ± 2σ		n=13			97.8	0.25	K$_2$O=0.95%		2.31	0.11
	Plateau ± 2σ	steps D-K	n=8	MSWD=1.40		90.1	0.26 ±0.07		92.1	1.727	0.050
	Isochron±2σ	steps C-M	n=11	MSWD=1.04			^{40}Ar/^{36}Ar=325.0±10.0			1.671	0.051

Notes:
- Isotopic ratios corrected for blank, radioactive decay, and mass discrimination, not corrected for interfering reactions.
- Errors quoted for individual analyses include analytical error only, without interfering reaction or J uncertainties.
- Integrated age calculated by summing isotopic measurements of all steps.
- Integrated age error calculated by quadratically combining errors of isotopic measurements of all steps.
- Plateau age is inverse-variance-weighted mean of selected steps.
- Plateau age error is inverse-variance-weighted mean error (Taylor, 1982) times root MSWD where MSWD>1.
- Plateau error is weighted error of Taylor (1982).
- Decay constants and isotopic abundances after Steiger & Jäger (1977).
- # symbol preceding sample ID denotes analyses excluded from plateau age calculations.
- Weight percent K$_2$O calculated from ^{39}Ar signal, sample weight, and instrument sensitivity.
- Ages calculated relative to FC-2 Fish Canyon Tuff sanidine interlaboratory standard at 28.02 Ma
- Decay Constant (LambdaK (total)) = 5.543e-10/a
- Correction factors:
  - (^{39}Ar/^{37}Ar)$_{Ca}$ = 0.00068 ± 2e-05
  - (^{36}Ar/^{37}Ar)$_{Ca}$ = 0.00028 ± 1e-05
  - (^{38}Ar/^{39}Ar)$_K$ = 0.013
  - (^{40}Ar/^{39}Ar)$_K$ = 0 ± 0.0004

The preliminary ^{40}Ar/^{39}Ar results provide ages for four stratigraphic intervals within the AND-1B core adding significant age constraints to the age model. A highly precise age for the upper core at 85.53–85.85 mbsf was obtained by analysis of single crystal and groups of two to three K-feldspar grains. Analysis of glass from the basaltic tephra interval spanning from approximately 112 to 145 mbsf, while not as precise as the K-feldspar age. does provide two other age-constraining points for the age model. These two samples bracket glacial surface erosion (GSE) 9 to GSE12 and help to determine the amount of time removed by erosion. The whole-rock lava sample is the least precise of all the analyses but does yield a statistically acceptable eruption age. Two of the three volcanic clasts, 1277.91-1277.95 and 1278.84–1278.87 mbsf, yielded ages within 2σ uncertainty of each other. The third volcanic clast (1279.00–1279.04 mbsf) yielded a mean age younger than the two other clasts providing a maximum depositional age for sediment at 1279.00 mbsf. In the future we hope to identify and ^{40}Ar/^{39}Ar-date additional volcanic horizons and clasts.

Tab. 5 - ^{40}Ar/^{39}Ar analytical data for 648.37–648.43 mbsf submarine lava flow.

	ID	Temp	^{40}Ar/^{39}Ar	^{37}Ar/^{39}Ar	^{36}Ar/^{39}Ar	^{39}ArK	K/Ca	^{40}Ar*	^{39}Ar	Age	±1σ
		(°C)			(x 10^{-3})	(x 10^{-15} mol)		(%)	(%)	(Ma)	(Ma)
	648-GM-HCl. Groundmass Concentrate. 51.89 mg. J=0.0006793±0.10%. D=1.002±0.001. NM-203C. Lab#=56788-01										
xi	A	625	1088.4	0.978	3389.9	4.13	0.52	8.0	6.6	103.3	4.9
	B	700	11.85	1.117	22.82	8.76	0.46	43.9	20.4	6.36	0.13
	C	750	8.227	1.282	10.53	7.86	0.40	63.5	32.9	6.39	0.13
	D	800	7.788	2.099	9.292	7.09	0.24	67.0	44.2	6.39	0.15
	E	875	7.500	1.409	7.533	11.58	0.36	71.9	62.5	6.600	0.093
	F	975	7.666	1.225	7.839	9.05	0.42	71.1	76.9	6.67	0.12
	G	1075	10.03	1.443	17.02	8.99	0.35	51.1	91.2	6.28	0.13
x	H	1250	11.60	7.004	21.88	4.88	0.073	49.3	98.9	7.02	0.22
x	I	1700	16.60	7.771	37.67	0.688	0.066	36.8	100.0	7.5	1.4
	Integrated age ± 2σ			n=9		63.0	0.27	K$_2$O=0.69%		13.03	0.73
	Plateau ± 2σ	steps B-G		n=6	MSWD=1.72	53.3	0.37 ±0.15		84.6	6.48	0.13
	Isochron±2σ	steps B-I		n=8	MSWD=2.40		^{40}Ar/^{36}Ar=289.8±13.7			6.59	0.22

Notes:
- Isotopic ratios corrected for blank. radioactive decay, and mass discrimination, not corrected for interfering reactions.
- Errors quoted for individual analyses include analytical error only, without interfering reaction or J uncertainties.
- Integrated age calculated by summing isotopic measurements of all steps.
- Integrated age error calculated by quadratically combining errors of isotopic measurements of all steps.
- Plateau age is inverse-variance-weighted mean of selected steps.
- Plateau age error is inverse-variance-weighted mean error (Taylor, 1982) times root MSWD where MSWD>1.
- Plateau error is weighted error of Taylor (1982).
- Decay constants and isotopic abundances after Steiger & Jäger (1977).
- # symbol preceding sample ID denotes analyses excluded from plateau age calculations.
- Weight percent K$_2$O calculated from ^{39}Ar signal, sample weight, and instrument sensitivity.
- Ages calculated relative to FC-2 Fish Canyon Tuff sanidine interlaboratory standard at 28.02 Ma
- Decay Constant (LambdaK (total)) = 5.543e-10/a
- Correction factors:
  - $(^{39}Ar/^{37}Ar)_{Ca}$ = 0.00068 ± 2e-05
  - $(^{36}Ar/^{37}Ar)_{Ca}$ = 0.00028 ± 1e-05
  - $(^{38}Ar/^{39}Ar)_{K}$ = 0.013
  - $(^{40}Ar/^{39}Ar)_{K}$ = 0 ± 0.0004

^{87}Sr/^{86}Sr AGES

The AND-1B drill core was inspected for calcareous macrofossils and microfossils suitable for strontium isotope dating using the marine ^{87}Sr/^{86}Sr curve. Although unevenly distributed, carbonate macrofossils were identified at many levels in the upper 600 m of the core. However, most of the extracted material is represented by taxonomically undetermined fragments, pertaining to either bivalves or cirriped crustaceans (barnacles). In some cases, it is uncertain whether the fragments are bivalve or barnacle (Tab. 7).

Strontium isotope ratios were determined on shell fragments from 16 different horizons between 91.55 and 473.62 mbsf in the drill core (Tab. 7). Analysis was carried out the University of Melbourne by Drs Jon Woodhead and Roland Maas. Ages were derived by adjusting measured ^{87}Sr/^{86}Sr values to SRM987 (^{87}Sr/^{86}Sr = 0.710248) and applying the Strontium Look-up Table (version 4:08/04) described in McArthur et al. (2001). Errors are quoted as 2-sigma (upper and lower) limits, taking into account measurement precision as well as statistical uncertainties on the compiled strontium isotope seawater curve.

The resulting ages (Tab. 7) cover a wide range. 4.8–19.5 Ma, and show no uniform trends downcore. The highest ages (9.75–19.50 Ma) are for bivalve fragments—the sample from 473.6 mbsf, which also has a high age, is only tentatively identified

as barnacle, and could be bivalve. The lowest ages (4.82–5.90 Ma) are for known or suspected barnacle fragments—the sample from 337.67 mbsf, which also has a low age, is only tentatively identified as bivalve. and could be barnacle.
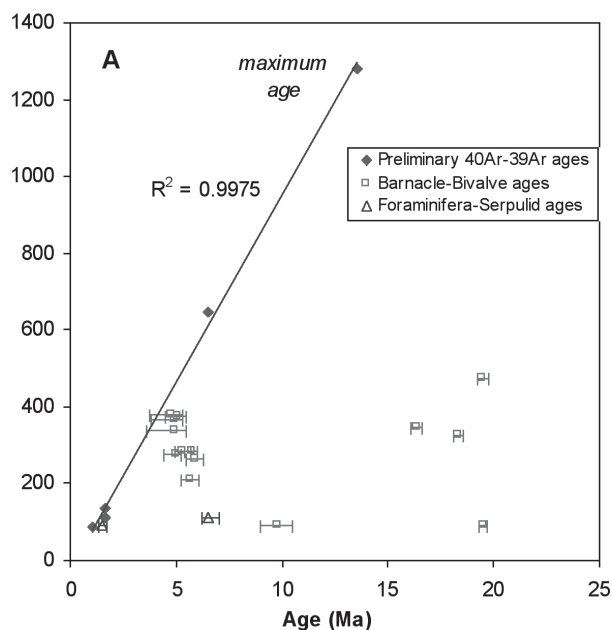

Fig. 2 – Strontium isotope ages for shell material from AND-1B. compared with a constant sedimentation rate curve derived from preliminary ^{40}Ar/^{39}Ar ages on volcanic material (least squares regression through five data points). Error bars are 2σ.

Tab. 6 - $^{40}Ar/^{39}Ar$ analytical data for ~1280 mbsf volcanic clasts.

ID	$^{40}Ar/^{39}Ar$	$^{37}Ar/^{39}Ar$	$^{36}Ar/^{39}Ar$	^{39}ArK	K/Ca	Cl/K	$^{40}Ar*$	Age	±1σ
			(x 10-3)	(x 10-15 mol)			(%)	(Ma)	(Ma)
1277-91. Sanidine. J=0.0007122±0.04%. D=1.002±0.001. NM-203D. Lab#=56793									
15	11.43	0.022	2.502	1.386	23.2	0.000	93.5	13.69	0.20
01	11.91	0.022	4.060	1.081	22.8	-0.000	89.9	13.71	0.26
13	11.24	0.018	1.762	1.536	28.1	-0.000	95.4	13.72	0.18
07	11.40	0.019	2.265	1.490	27.0	-0.000	94.1	13.74	0.19
03	12.56	0.017	6.165	1.416	30.3	-0.000	85.5	13.75	0.20
06	11.15	0.024	1.404	1.237	21.6	-0.000	96.3	13.75	0.22
12	11.10	0.022	1.234	2.162	22.9	-0.000	96.7	13.75	0.13
08	11.78	0.023	3.344	1.626	21.8	-0.000	91.6	13.82	0.17
14	11.08	0.018	0.852	1.709	27.8	-0.000	97.7	13.86	0.16
09	11.05	0.013	0.731	1.573	39.9	-0.000	98.1	13.86	0.18
04	11.09	0.008	0.870	0.949	65.5	-0.000	97.7	13.87	0.29
11	11.09	0.021	0.856	2.949	24.0	0.000	97.7	13.869	0.097
05	11.49	0.019	2.165	0.968	26.3	-0.001	94.4	13.90	0.29
02	11.09	0.008	0.498	0.974	66.8	-0.000	98.7	14.01	0.28
10	12.24	0.031	4.118	0.996	16.5	-0.000	90.1	14.12	0.28
Mean age ± 2σ	n=15	MSWD=0.26		31.0 ±30.4				13.816	0.093
1278-84, Sanidine, J=0.0007111±0.04%, D=1.002±0.001, NM-203D, Lab#=56794									
10	11.03	0.003	2.088	0.473	192.0	0.000	94.4	13.31	0.59
07	11.00	0.003	1.327	1.269	148.7	-0.000	96.4	13.55	0.22
08	11.11	0.005	1.658	0.774	94.2	0.000	95.6	13.57	0.35
12	11.21	-0.002	1.676	0.546	-	0.000	95.6	13.69	0.52
11	11.24	0.016	1.613	0.925	31.9	-0.000	95.8	13.76	0.30
13	11.39	-0.005	2.018	0.292	-	0.001	94.8	13.8	1.0
03	11.21	0.012	1.259	0.885	43.9	-0.000	96.7	13.85	0.30
05	10.97	0.001	0.401	0.811	341.7	0.000	98.9	13.87	0.33
02	11.26	0.000	1.287	0.528	20740.0	0.001	96.6	13.91	0.51
04	11.34	0.004	1.502	0.592	131.6	0.000	96.1	13.93	0.46
06	11.55	0.001	2.038	1.109	402.1	-0.000	94.8	13.99	0.24
01	10.98	0.007	-0.049	1.430	68.7	-0.000	100.1	14.06	0.19
14	12.30	0.015	4.178	0.413	33.2	-0.000	90.0	14.15	0.71
09	11.11	0.018	0.092	0.666	27.8	-0.000	99.8	14.17	0.41
Mean age ± 2σ	n=14	MSWD=0.45		1854.7±11014.7				13.85	0.18
1279-00, Sanidine, J=0.0007135±0.04%, D=1.002±0.001, NM-203D, Lab#=56792									
01	11.24	0.062	3.154	0.939	8.3	0.000	91.8	13.23	0.33
05	10.98	0.046	2.172	0.638	11.1	0.001	94.2	13.27	0.45
06	10.88	0.076	1.292	1.215	6.7	-0.000	96.5	13.47	0.24
02	10.84	0.066	1.148	1.968	7.7	-0.000	96.9	13.48	0.16
03	11.00	0.058	1.650	1.767	8.8	0.000	95.6	13.49	0.17
10	10.94	0.070	1.362	1.069	7.3	0.000	96.4	13.52	0.26
15	11.05	0.089	1.716	0.642	5.7	0.000	95.5	13.53	0.43
04	11.03	0.061	1.523	2.473	8.4	-0.000	96.0	13.57	0.12
08	11.02	0.067	1.238	0.708	7.6	-0.000	96.7	13.67	0.39
12	11.26	0.055	1.911	1.015	9.2	0.000	95.0	13.72	0.27
07	11.74	0.063	3.410	0.864	8.1	0.000	91.5	13.77	0.32
13	11.09	0.063	1.095	0.697	8.1	-0.000	97.1	13.82	0.39
09	11.32	0.072	1.455	0.744	7.1	0.000	96.3	13.97	0.37
14	10.99	0.060	0.158	0.641	8.5	-0.001	99.6	14.04	0.42
11	10.80	0.028	-0.562	0.621	18.3	-0.000	101.6	14.06	0.44
Mean age ± 2σ	n=15	MSWD=0.51		8.7 ±5.8				13.57	0.13

Notes:
- Isotopic ratios corrected for blank, radioactive decay, and mass discrimination, not corrected for interfering reactions.
- Errors quoted for individual analyses include analytical error only, without interfering reaction or J uncertainties.
- Mean age is weighted mean age of Taylor (1982). Mean age error is weighted error of the mean (Taylor, 1982). multiplied by the root of the MSWD where MSWD>1, and also incorporates uncertainty in J factors and irradiation correction uncertainties.
- Decay constants and isotopic abundances after Steiger & Jäger (1977).
- # symbol preceding sample ID denotes analyses excluded from mean age calculations.
- Ages calculated relative to FC-2 Fish Canyon Tuff sanidine interlaboratory standard at 27.84 Ma
- Decay Constant (LambdaK (total)) = 5.543e-10/a
- Correction factors:
    - $(^{39}Ar/^{37}Ar)_{Ca}$ = 0.00068 ± 2e-05
    - $(^{36}Ar/^{37}Ar)_{Ca}$ = 0.00028 ± 1e-05
    - $(^{38}Ar/^{39}Ar)_{K}$ = 0.013
    - $(^{40}Ar/^{39}Ar)_{K}$ = 0 ± 0.0004

Tab. 7 - Strontium isotope ages for shell material from AND-1B. Age limits are 2-sigma.

Depth in Core (mbsf)	Type	Age (Ma)	Lower limit (Ma)	Upper Limit (Ma)
91.55-91.61	Bivalve	9.78	9.00	10.46
91.56-91.61	Foraminifera – small	1.52	1.46	1.57
91.71-91.73	Bivalve	19.50	19.29	19.72
110.98-111.03	Serpulid – large	6.51	6.43	6.59
211.32-211.35	Barnacle?	5.71	5.23	6.03
265.48-265.51	Barnacle?	5.90	5.47	6.25
276.20-276.23	Barnacle? – large	4.99	4.44	5.23
284.97-285.00	Barnacle? – large	5.75	5.42	6.00
285.85	Barnacle	5.34	4.91	5.68
325.05-325.07	Bivalve	18.34	18.09	18.57
337.66-337.68	Bivalve?	4.93	3.60	5.43
345.05-345.08	Bivalve?	16.38	16.12	16.59
365.00-365.05	Barnacle? – small	4.93	3.82	5.31
374.21-374.23	Barnacle – large	5.09	4.50	5.46
378.02-378.07	Barnacle – large (1 cm)	4.82	3.73	5.30
473.61-473.62	Barnacle? – small	19.47	19.21	19.75

The youngest ages are within error of a constant sedimentation-rate curve derived from preliminary $^{40}Ar/^{39}Ar$ geochronology (Fig. 2), and could be valid. However, many of the ages are significantly higher than this curve, and outside the broad age boundaries defined by diatom biostratigraphy.

These discrepancies from the expected ages might be explained in four ways, none of which are mutually exclusive:

1. Recycling of fossil material from older horizons;
2. Local reductions in the $^{87}Sr/^{86}Sr$ of seawater (due to proximity to glacial outwash flows);
3. Partial re-equilibration of primary $^{87}Sr/^{86}Sr$ with less-radiogenic pore fluids via calcite deposition on shell surfaces, or diffusive exchange; or
4. Contamination of primary $^{87}Sr/^{86}Sr$ by less-radiogenic matrix sediment.

Some effort was made to determine which of the above four explanations are more likely to contribute to the age discrepancies. and to improve the quality of the measured ages through sequential etching. All of the original samples contained various amounts of mud adhered to surfaces or trapped in pores, suggesting that explanation number 4 was the prime suspect. Hence, all samples were initially ultrasonicised in distilled water, then some were mildly etched in cold, distilled 0.2 M HCl for 10 minutes, followed by variable etching in cold distilled 0.5 M HCl for 5 minutes to loosen and remove adhered mud (this would also remove redeposited surface calcite if present). Strontium was then extracted using doubly distilled 1.6 M acetic acid at 50°C and analysed for its isotopic composition.

After the initial results were obtained, additional samples from four of the horizons were subjected to multiple etching cycles. The results (Tab. 8; Fig. 3) were equivocal. with little general improvement in the derived ages. A mixed foraminiferal sample obtained by Percy Strong from *c.* 91.6 mbsf yielded an age consistent with nearby $^{40}Ar/^{39}Ar$ results

(Fig. 2), whereas a serpulid from *c.* 111 mbsf yielded a spuriously high age (because of the more delicate nature of these samples, a single etching step using 0.5 M HNO_3 was undertaken).

The extremely variable ages for several different bivalve fragments, as well as the foraminiferal sample from the same general horizon at *c.* 91.6 mbsf, counts against recycling, unless each of the samples were derived from beds of very different age ranging back to the mid-Oligocene. The same goes for the barnacle fragments from *c.* 365 mbsf and, to a lesser degree, from *c.* 276.2 mbsf. The *c.* 19.5 Ma age for the possible barnacle fragment from 473.6 mbsf, if it is indeed barnacle, is considered highly unlikely. Also, the barnacles generally (perhaps exclusively) yielded
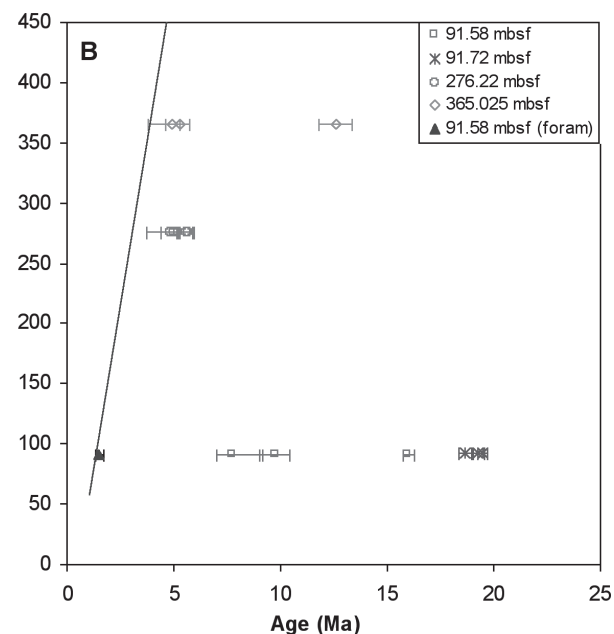

Fig. 3 – Strontium isotope ages of shell material from AND-1B after sequential leaching. compared with $^{40}Ar/^{39}Ar$ ages on volcanic material (least squares regression through three data points—*c.* 113. 136 & 648 mbsf). Error bars are 2σ.

Tab. 8 - Strontium isotope ages and etching details for selected macrofossil samples

Sample	Type	Fragment	Age (Ma)	0.2M HCl	0.5M HCl	0.5M HCl	0.5M HCl	0.5M HCl
91.55-91.61*	Bivalve	1-A	9.78					
91.55-91.61	Bivalve	2	15.97	X	X			
91.55-91.61*	Bivalve	1-B	7.78	X	X			
91.71-91.73*	Bivalve	1-A	19.50					
91.71-91.73*	Bivalve	1-B	19.27	X	X			
91.71-91.73*	Bivalve	1-C	18.65	X	X			
276.20-276.23	Barnacle?	1-A	4.99					
276.20-276.23	Barnacle?	1-B	5.67	X	X	X	X	X
276.20-276.23#	Barnacle?	1-C	4.82	X	X	X		
276.20-276.23#	Barnacle?	1-D	5.61	X	X			
365.00-365.05	Barnacle?	1	4.93					
365.00-365.05	Barnacle?	2	12.58	X	X			
365.00-365.05	Barnacle?	3	5.28	X	X	X	X	X

* brown patches remained after etching # minor adhered mud remained after etching
A, B, C or D are different splits of the same original fragment; 1, 2 or 3 are different fragments from the same horizon

the youngest ages, yet are generally considered more prone to reworking than the bivalves.

The variable ages derived for the same horizons does, however, rule out local variation in seawater $^{87}Sr/^{86}Sr$, since all samples at any horizon should yield the same, albeit incorrect strontium isotope age.

Partial re-equilibration of strontium isotopes via circulating pore fluids is a possibility that cannot be ruled out, despite a lack of strong microscopic evidence for re-crystallisation or calcite deposition on the analysed samples. After successive leaching, most of the samples had fresh, smooth surfaces, except for a few (marked with an asterisk in Tab. 8) that retained some brownish patches, which are assumed to be organic matter; those samples yielded strontium isotope ages that overlapped with the other, pristine samples from the same horizon. Partial equilibration with pore-fluid strontium might explain the lower ages for the barnacle fragments, which are considered to be more resistant to such processes than the bivalves.

Whereas recycling and re-equilibration both might play a role in producing the spurious high strontium isotope ages for macrofossils, it seems certain that contamination by mud from the host sedimentary matrix has played a significant role. As illustrated by the results in table 8, the mud would have to have a strong buffering effect (high strontium with a relatively low $^{87}Sr/^{86}Sr$, presumably derived from local volcanic ash) to produce such widely varying results for the samples irrespective of their apparent degree of 'cleanliness'—for example. the lowest strontium isotope age for barnacle fragments from *c.* 276.2 mbsf is yielded by a sample that, after several etchings, still retained some surface mud, and not by the 'clean' sample that was subjected to an additional etching step (Tab. 8). Clearly, mud retained in subsurface cavities must continue to have a significant influence on derived ages even after several cycles of etching with dilute HCl.

Several solutions to the dating problem present themselves:

1. Apply an even more protracted cleaning process to the freshest-looking shell fragments. As illustrated in figure 3, such a procedure may still not remove silicate material in deep pores or sub-surface coatings. Hence, there will always be a question mark over the validity of the derived ages.

2. Drill the centres of the largest shell fragments. if any can be found that are sufficiently large. This has the potential to avoid obviously contaminated areas. but still provides no guarantee of success due to possible hidden pores or cavities. It might, however, lay to rest the possibility of recycling being the main factor in producing the spurious ages.

3. Apply laser ablation micro-sampling by ICP-MS to clean shell surfaces. Individually, this would yield only 50% of TIMS precision, but that can be improved by statistically pooling data from several runs. Also, core-to-rim traverses might serve to highlight contamination gradients, improving the certainty of the final result.

4. Use only foraminifera. The one foraminifera sample analysed so far yielded a result that is broadly consistent with adjacent $^{40}Ar/^{39}Ar$ data—this sample contained a relatively large amount of foreign material (brownish mud or organics. glassy crystallites) but, after light crushing, sufficient (*c.* 2 mg) fresh material was extracted to yield a precise analysis. The problem is that foraminifera are scarce within the core. making the accumulation of samples of 3–4 mg difficult to achieve—this sample size is required due to attrition resulting from the necessary crushing and handpicking step. A possible way around this is to laser-ablate individual foraminifera tests, using ICP-MS. The technical viability of this is presently under investigation.

GLACIAL SURFACES OF EROSION

A total of 41 glacial surfaces of erosion (GSE) were identified in the upper 700 m of the AND-1B

drill core during initial core characterisation (Krissek et al., this volume). These surfaces record a period of glacial advance that resulted in erosion of underlying strata. and hence potentially represent hiatuses in the succession. GSEs are identified on the basis of sharp facies dislocations, which in some cases may be amalgamated, that separate diamictite from underlying facies, which can vary widely in character. The underlying deposits are often sheared and display soft-sediment deformation and physical mixing of lithologies. Where an advance of grounded ice is represented by a diamictite that overlies another diamictite, the GSE is difficult to identify due to the amalgamation of the two. In such cases, the GSE is defined based on the facies sequence below, which may include deformed and physically mixed intervals, and/or the overlying diamictite that may contain soft-sediment mudstone and diamictite intraclasts. However, in most cases where diamictites are amalgamated, variability in the degree of stratification allows fluctuations in the grounding line to be recognised. The predominance of proximal subglacial and proglacial coarse-grained facies in the Pleistocene interval (upper 100 m. *e.g.* LSU 1.1; 0–82.74 mbsf) suggests (1) that the cycles are significantly truncated with distal interglacial and subsequent proglacial facies removed, or (2) a long period dominated by a grounded ice sheet with glacimarine facies incursions only occurring at interglacial minima. That numerous fluctuations in the grounding line do occur in the upper diamictite succession above 85 m suggests a condensed, but relatively complete stratigraphic record with time lost periodically at glacial maxima within GSEs.

MAGNETOSTRATIGRAPHY

Characteristic remanence directions were identified at metre resolution between 32 and 240 mbsf and at 2 m resolution between 240 and 700 mbsf in the AND-1B drill core (see G. Wilson et al. this volume). The inclination data define a series of 15 magnetozones (9 normal and 8 reversed polarity) of alternating polarity between 32 and 700 mbsf in the drill core, with roughly equal normal and reversed polarity represented. Most magnetozone boundaries are well defined in the drill core and picked at the midpoint between samples of opposing polarity no more than 2 m apart or at transitional polarity samples. Polarity interpretation in the upper 200 m is relatively straightforward, with the highest normal magnetozone (above 80.03 mbsf; N1) correlated with the Brunhes Normal Chron and the long reversed magnetozone between 91.13 and 191.75 mbsf (R2) correlated with part of the Matuyama Reversed Chron, and with the polarity boundary at 191.75 mbsf (MPR4) recognised as the Gauss/Matuyama boundary. Polarity interpretation of the interval between 400 and 600 mbsf is also relatively straightforward with a one-to-one match of the N4-R4-N5-R5-N6 polarity pattern with

polarity subchrons C3n.1n-C3n.1r-C3n.2n-C3n.2r-C3n.3n of the Gilbert reversed chron. Given fewer independent constraints. the frequency of erosion surfaces in the core and the highly variable facies and potential sedimentation rates in the remaining intervals above 700 mbsf (200–400 mbsf and below 600 mbsf) in the AND-1B drill core, correlation of the magnetic polarity stratigraphy with the GPTS is ambiguous and several correlation options are possible. One exception is Magnetozone R7, which is correlated with Subchron C3An.1r as it contains the basaltic lava flow ^{40}Ar/^{39}Ar dated at 6.48 ± 0.09. At the time of writing, magnetic polarity had not been determined for the lower part of the core (700–1284.87 mbsf).

CONSTRUCTION OF THE AGE MODEL

Diatom first and last occurrences (D) are plotted on figure 4 according to a constrained optimisation model for Southern Ocean diatom biochronology and published age ranges as summarised by Cody et al. (2007). Left-facing arrows represent first occurrences and right-facing arrows represent last occurrences, respectively. Fine vertical dashed lines represent potential error in identification in the occurrences in the AND-1B core either from possible reworking or sporadic occurrences. Yellow boxes represent age and depth range of diatom unit assemblages (DUA) from diatomaceous intervals in the core. Age ranges for assemblage units are derived from published data summarised in Cody et al. (2007). ^{40}Ar/^{39}Ar ages (A) are plotted as red dots with error bars on figure 4 – only A4 has a significant error. The strontium age on foraminifera from 91.56–91.61 mbsf is plotted as a beige dot with error bars. Lines Ri, Rj, and Rk represent seismic reflection horizons identified in seismic reflection data. Potential disconformities in accumulation are shown on figure 4, primarily, where glacial surfaces of erosion were identified by physical criteria observed in the drill core.

Correlation of the magnetozones identified in the AND-1B core with the GPTS (Ogg & Smith 2004) is constrained as follows: (1) Line of correlation is pinned to ^{40}Ar/^{39}Ar ages within errors and matching polarity; (2) line of correlation is constrained by age range of diatom assemblage zones and matching polarity; (3) line of correlation passes younger than individual first occurrences and older than individual last occurrences where these are consistent with diatom assemblage zones; (4) Solid line of correlation is drawn where a 1:1 match of polarity stratigraphy with the GPTS is defined, recognized polarity reversals are marked with a plus (+); (5) a dashed line of correlation represents upward or downward continuation to the nearest disconformity within polarity constraints but where other constraints do not preclude alternative polarity correlations; (6) no line of correlation is given for intervals with multiple disconformities and limited constraints.
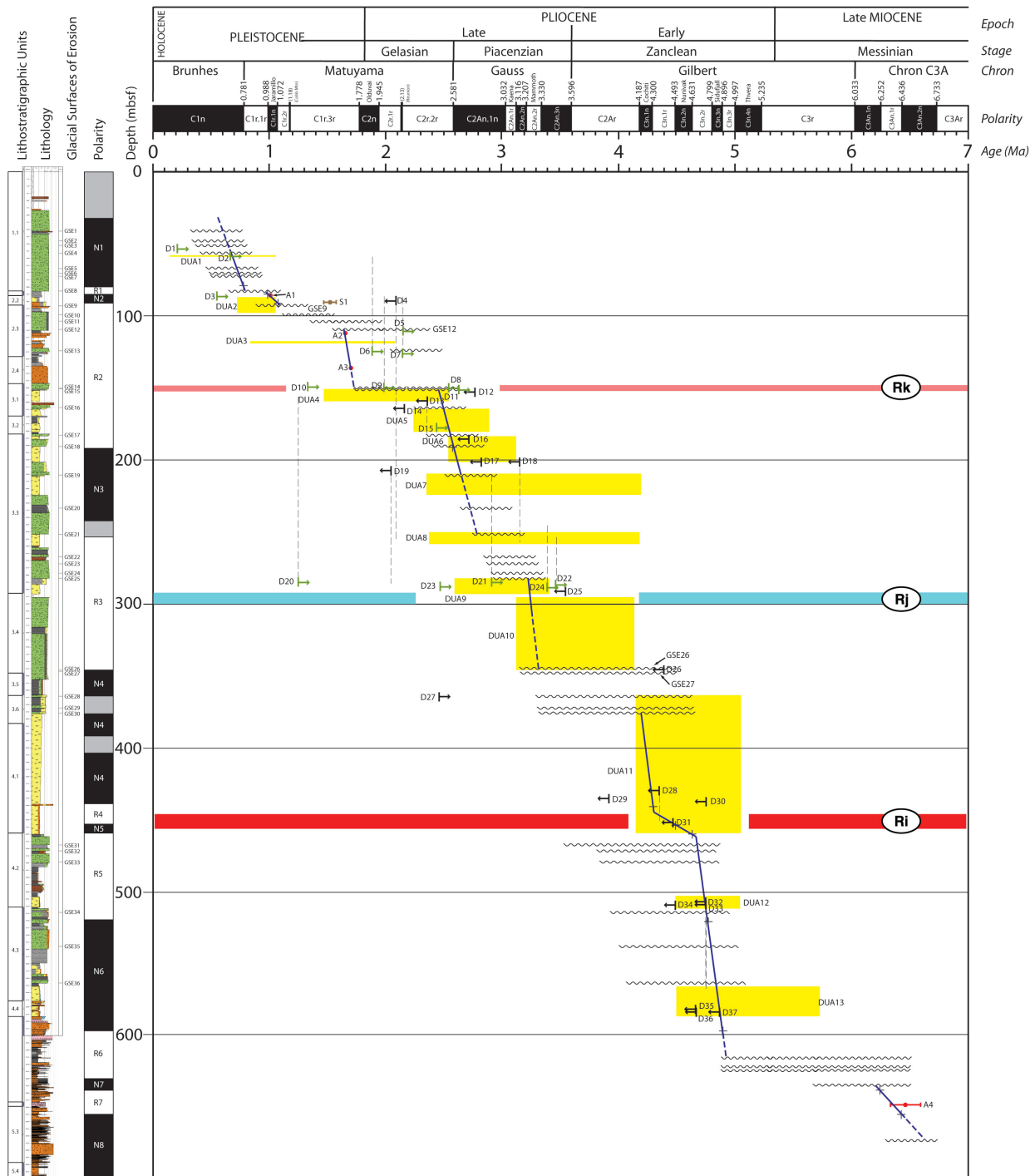
Fig. 4 – Preliminary age model for the upper 700 m of the AND-1B drill core. The age model is based on diatom biostratigraphy (D = individual first and last occurrence datums. DUA = Diatom assemblage zones). $^{40}Ar/^{39}Ar$ ages (A) on tephric material. $^{87}Sr/^{86}Sr$ (S) analyses of foraminifera and magnetostratigraphy. Disconformities represent glacial surfaces of erosion. Ri. Rj. and Rk are seismic reflection horizons identified by the seismic reflection data. Line of correlation to the Geomagnetic Polarity Time Scale (Ogg & Smith 2004) is shown as solid with polarity reversal tiepoints marked with a '+' where other constraints allow a unique correlation and is dashed where continuity of accumulation is inferred. No line of correlation is given for intervals with multiple disconformities and limited constraints.

THE PLEISTOCENE RECORD (0–150 mbsf)

The diatom assemblages between 52.98 and 97.08 mbsf (DUA1 and DUA2) indicate that the AND-1B core is younger than 1.07 Ma above 97.08 mbsf. which is confirmed by the $^{40}Ar/^{39}Ar$ age of 1.014 ± 0.004 Ma on the pumice at 85.50 mbsf. Accordingly, the long normal magnetozone above 80.03 mbsf (N1) is correlated with the Brunhes Normal Chron (C1n) and the short normal magnetozone between 84.97 and 91.13 mbsf with the Jaramillo Subchron (C1r.1n). The base of the Brunhes Normal Chron (C1n) is assigned an age of 0.781 Ma and the Jaramillo Subchron (C1r.1n) is assigned an age range of 0.988–1.072 m.y. by Ogg & Smith (2004). The age of the top of normal magnetozone N1 is relatively unconstrained and it is therefore not possible to

indicate sedimentation rates with any accuracy. The seven glacial surfaces of erosion identified in the diamictite of lithostratigraphic subunit 1.1 indicate a punctuated rather than continuous record of accumulation, with potential erosion during glacial maxima. The short reversed polarity magnetozone (R1) is correlated with Subchron C1r.1r; however, its relative thinness may suggest a slow sedimentation rate, or a hiatus on the order of 100 k.y. at the Glacial Surface of Erosion at 82.74 mbsf (GSE8). The top of the reversed magnetozone below 91.13 mbsf is correlated with Subchron C1r.2r.

Two $^{40}Ar/^{39}Ar$ ages on basaltic tephra constrain the interval reversed polarity between 112.51 and 136.21 mbsf to the lowermost Pleistocene (lower part of polarity subchron C1r.3r; 1.65–1.67 Ma) and suggest a relatively rapid sediment accumulation rate in this interval of the drill core. A series of glacial surfaces of erosion between 93.00 and 109.42 mbsf accounts for much of the early Pleistocene (Subchron C1r.3r). A significant hiatus (1.7-2.4 m.y.) that is co-incident with the Rk seismic reflector separates the Pleistocene diamictite succession from the underlying Pliocene succession of alternating diamictites and diatomites. The hiatus coincides with a closely spaced pair of glacial erosion surfaces (GSE 13 and GSE 14) and accounts for the Pliocene/Pleistocene boundary as well as the Olduvai (C2n) Chron.

THE LATE PLIOCENE RECORD (150–~350 mbsf)

The diatom assemblage between 150.87 and 201.59 mbsf in the AND-1B core (DUA4–DUA6) suggests that this interval spans the Gauss (Subchron C2An.1n)/Matuyama (Subchron C2r.2r) boundary. Accordingly, the lower part of Magnetozone R2 and the upper part of Magnetozone N3 are correlated with subchrons C2r.2r and C2An.1n, respectively and an age of 2.581 Ma (Ogg & Smith 2004) is assigned to the polarity reversal at 191.75 mbsf in the AND-1B drill core. Between 283.35 and 346.94 mbsf, diatom assemblage zones DUA9 and DUA10 suggest that the reversed-polarity (Magnetozone R3) between GSE 25 (282.23 mbsf) and GSE 26 (345.95 mbsf) part of reversed polarity magnetozone R3. correlates with Subchron C2An.2r. This interval also contains the Rj seismic reflector co-incident with a lithologically distinct diamictite – diatomite transition in lithostratigraphic subunit 3.4 with no hiatus indicated. While unambiguous correlation is not possible for the rest of the upper Pliocene interval of the core. an average sediment accumulation rate of 0.2 m/k.y. with Milankovitch-order cyclicity in diatomite/diamictite alternations is suggested.

EARLY PLIOCENE RECORD (~350–~620 mbsf)

A succession of disconformities between 346.03 and 375.85 mbsf contain the lower/upper Pliocene boundary with a 0.5–1 m.y. hiatus distributed on one or more of the glacial surfaces of erosion (GSE26–GSE30). Between 363.37 and 586.45 mbsf, diatom flora (DUA11, DUA12, and DUA13) constrain correlation of this interval of the AND-1B drill core with the latest Miocene–early Pliocene (5.7–4.16 Ma). Within these constraints, a unique correlation is possible between magnetozones N4-R4-N5-R5-N5 and polarity subchrons C3n.1n-C3n.1r-C3n.2n-C3n.2r-C3n.3n, respectively. An average sediment accumulation rate of 0.5 m/k.y. is indicated for both the mostly diatomaceous intervals as well as the alternating diamictite/diatomite intervals, with one exception; the lower part of diatomaceous lithostratigraphic subunit 4.1. where a much slower sediment accumulation rate (~0.1 m/k.y.) is indicated. This interval corresponds with seismic reflection horizon Ri. An age of 5.0 Ma is indicated at 600 mbsf in the AND-1B drill core.

THE MIOCENE RECORD (>~620 mbsf)

A series of hiatuses between 615.50 and 635.00 mbsf (GSE37–GSE 40) encompasses the Miocene/Pliocene boundary and accounts for ~ 1 m.y. of time including Subchron C3n.4n and most of Chron C3r. An $^{40}Ar/^{39}Ar$ age (6.48 ± 0.13 Ma) on the basaltic lava flow at 648.37–648.43 mbsf indicates a late Miocene age for this interval of the core and a correlation between reversed-polarity magnetozone R7 and Chron C3A is implied. At the time of writing, the only chronostratigraphic data available below 700 mbsf include three $^{40}Ar/^{39}Ar$ ages (13.82 ± 0.09 Ma. 13.85 ± 0.18 Ma. and 13.57 ± 0.13 Ma) on volcanic clasts from near 1280 mbsf. affording a maximum depositional age for the base of the AND-1B drill core.

AGE MODEL SUMMARY FOR 0–600 mbsf IN AND-1B

Integrated chronostratigraphic data comprising diatom assemblages and datums, $^{40}Ar/^{39}Ar$ ages on volcanic material, and magnetostratigraphy constrain a preliminary age model for the upper 700 m of the AND-1B drill core. Diatom assemblages and datums are distributed through the core between 52.98 and 586.45 mbsf and provide a 0.5 to 1–2 m.y. resolution age constraint. Magnetostratigraphic constraint is also available between 32.33 and 700 mbsf with metre spaced samples between 32.33 and 240 mbsf and 2 m spaced samples between 240 and 700 mbsf.

$^{40}Ar/^{39}Ar$ ages at 85.50 mbsf, 112.51 mbsf, 136.21 mbsf, and 648.37 mbsf, respectively provide additional constraints at those levels and allow a higher resolution line of correlation in the age model. Glacial surfaces of erosion are identified throughout the core and indicate a punctuated rather than continuous rate of sediment accumulation.

Between 50 and 100 mbsf, the base of the Brunhes Normal Chron (C1n) and the Jaramillo Subchron (C1r.1n) are identified and provide good constraint on the age model. The identification of the Jaramillo Subchron is confirmed by a precise $^{40}Ar/^{39}Ar$ age (1.014 ± 0.004 Ma). Between 93.00 and 109.42 mbsf several erosion surfaces account for a ~0.5 m.y. hiatus. Between 112.51 and 136.21 mbsf, sediment accumulation was rapid with less than 0.1 m.y. of the lowermost Pleistocene (Subchron C1r.3r) represented. The Pliocene/Pleistocene boundary and the Olduvai (Chron C2n) occur within a ~1 m.y. hiatus which coincides with seismic reflection horizon Rk. Diatom flora between 150.87 and 201.59 mbsf constrain this interval to the late Pliocene and allow the identification of the Gauss (C2An.1n)/Matuyama (C2r.2r) boundary (2.581 Ma) at 191.75 mbsf in the drill core. While unambiguous correlation is not possible for the rest of the upper Pliocene interval of the AND-1B drill core, an average sediment accumulation rate of 0.2 m/k.y. with Milankovitch-order cyclicity in diatomite/diamictite alternations is suggested.

A succession of disconformities between 346.03 and 375.85 mbsf contain the lower/upper Pliocene boundary with a 0.5–1 m.y. hiatus distributed on one or more of the glacial surfaces of erosion. Between 363.37 and 586.45 mbsf, diatom flora constrains correlation of this interval of the AND-1B drill core with the latest Miocene–early Pliocene (5.7–4.16 Ma). An average sediment accumulation rate of 0.5 m/k.y. is indicated for both the mostly diatomaceous intervals as well as the alternating diamictite/diatomite intervals.

A series of hiatuses between 615.50 and 635.00 mbsf encompass the Miocene/Pliocene boundary and account for ~1 m.y. of time and a $^{40}Ar/^{39}Ar$ age (6.48 ± 0.13 Ma) on the basaltic lava flow at 648.37–648.43 mbsf indicates a late Miocene age for this interval of the core. At the time of this writing. the only chronostratigraphic data available below 700 mbsf include three $^{40}Ar/^{39}Ar$ ages on volcanic clasts from near 1280 mbsf affording a maximum depositional age of 13.57 Ma for the base of the AND-1B drill core.

REFERENCES

Baldauf J.G. & Barron J.A., 1991. Diatom Biostratigraphy: Kerguelen Plateau and Prydz Bay Regions of the Southern Ocean. In: Barron J.A.. Larsen B.. et al. (eds.). *Proceedings of the Ocean Drilling Program. Scientific Results*. College Station. TX (Ocean Drilling Program), **119**, 547–598.

Barron J.A., Baldauf J.G., Barrera E., Caulet B.T., Huber B.T., Keating B.H., Lazarus D., Sakai H., Thierstein H.R., & Wei W., 1991. Biochronologic and Magnetochronologic Synthesis of Leg 119 Sediments from the Kerguelen Plateau and Prydz Bay. Antarctica. In: Barron J.A.. Larsen B.. et al. (eds.). *Proceedings of the Ocean Drilling Program. Scientific Results*. College Station. TX (Ocean Drilling Program), **119**, 813–847.

Bohaty S.M., Scherer R.P. & Harwood D.M.. 1998. Quaternary Diatom Biostratigraphy and Palaeoenvironments of the CRP-1 Drillcore. Ross Sea. Antarctica. *Terra Antarctica*, **5**, 431–453.

Bohaty S.M., Wise S.W. Jr., Duncan R.A., Moore C.L. & Wallace P.J., 2003. Neogene Diatom Biostratigraphy. Tephra Stratigraphy. and Chronology of ODP Hole 1138A. Kerguelen Plateau. In: Frey F.A.. Coffin M.F.. Wallace P.J.. & Quilty P.G. (eds.). *Proceedings of the Ocean Drilling Program. Scientific Results*. College Station. TX (Ocean Drilling Program), **183**, 1–48.

Burckle L.H., Gartner S., Opdyke N.D., Sciarrillo J.R. & Shackleton N.J.,1978. Paleomagnetics. Oxygen Isotopes and Biostratigraphy of a Late Pliocene Section from the Central Pacific. In: Ikebe N. [chairperson]. *Correlation of Tropical through High Latitude Marine Neogene Deposits of the Pacific Basin*. Stanford University Publications: Geological Sciences, **14**, 10–11.

Censarek B. & Gersonde R., 2002. Miocene Diatom Biostratigraphy at ODP Sites 689. 690. 1088. 1092 (Atlantic sector of the Southern Ocean). *Marine Micropaleontology*, **45**, 209–256.

Censarek B. & Gersonde R., 2003. Data Report: Relative Abundance and Stratigraphic Ranges of Selected Diatoms from Miocene Sections at ODP Sites 689. 690. 1088. and 1092 (Atlantic Sector of the Southern Ocean). In: Gersonde R., Hodell D.A., & Blum P. (eds.), *Proceedings of the Ocean Drilling Program. Scientific Results*. College Station. TX (Ocean Drilling Program), **177** [Online].

Ciesielski P.F., 1983. The Neogene and Quaternary Diatom Biostratigraphy of Subantarctic Sediments. Deep Sea Drilling Project Leg 71. In: Ludwig W.J.. Krasheninikov V.A.. et al. (eds.). *Initial Reports of the Deep Sea Drilling Project*. Washington. DC. US Govt. Printing Office., **71**, 635–665.

Ciesielski P.F., 1991. Relative Abundances and Ranges of Select Diatoms and Silicoflagellates from Sites 699 and 704. Subantarctic South Atlantic. In: Ciesielski P.F.. Kristoffersen Y.. et al. (eds.). *Proceedings of the Ocean Drilling Program. Scientific Results*. College Station. TX (Ocean Drilling Program). **114**. 753–758.

Cody R.D., Levy R.H., & Harwood D. M., 2007. Thinking Outside the Zone: High Resolution Quantitative Diatom Biochronology for the Antarctic Neogene. *Palaeogeogr., Palaeoclim., Palaeoecol.,* in press.

Cooper R.A., Crampton J.S., Raine J.I.., Gradstein F.M., Morgans H.E.G., Sadler P.M., Strong C.P.., Waghorn D. & Wilson G.J., 2001. Quantitative Biostratigraphy of the Taranaki Basin. New Zealand: A Deterministic and Probabilistic Approach. *AAPG Bulletin*, **85**, 1469–1498.

Fenner J., 1991. Late Pliocene-Quaternary Quantitative Diatom Stratigraphy in the Atlantic Sector of the Southern Ocean. In: Ciesielski P.F., Kristoffersen Y., et al. (eds.), *Proceedings of the Ocean Drilling Program, Scientific Results,* College Station, TX (Ocean Drilling Program), **114**, 97–121.

Gersonde R. & Bárcena M.A., 1998. Revision of the Upper Pliocene-Pleistocene Diatom Biostratigraphy for the Northern Belt of the Southern Ocean. *Micropaleontology*, **44**, 84–98.

Gersonde R. & Burckle L.H., 1990. Neogene Diatom Biostratigraphy of ODP Leg 113. In: Barker P.F., Kennett J.P., et al. (eds.), *Proceedings of the Ocean Drilling Program, Scientific Results*. College Station, TX (Ocean Drilling Program), **113**, 761–789.

Harwood D.M. & Maruyama T., 1992. Middle Eocene to Pleistocene Diatom Biostratigraphy of Southern Ocean Sediments from the Kerguelen Plateau, Leg 120. In: Wise S.W. Jr., Schlich R., et al. (eds.), *Proceedings of the Ocean Drilling Program, Scientific Results,* College Station, TX (Ocean Drilling Program), **120**, 683–733.

Krissek L., Browne G., Carter L., Cowan E., Dunbar G., McKay R., Naish T., Powell R., Reed J. & Wilch T., this volume. Sedimentology and Stratigraphy of AND-1B core. ANDRILL McMurdo Ice Shelf Project. Antarctica. *Terra Antartica*.

Mahood & Barron, 1996. Late Pliocene Diatoms in a Diatomite from Prydz Bay. East Anatrctica. *Micropaleontology*, **42**, 285-302.

McArthur J.M., Howarth R.J. & Bailey T.R., 2001. Strontium Isotope Stratigraphy: A Robust LOWESS fit to the marine Sr-isotope Curve for 0 to 509 Ma and Accompanying Look-up Table for Deriving Numerical Age 'Look-Up Table Version 4:08/04'. *J. Geol.,* **109**, 155–169.

McCollum D.W., 1975. Diatom Stratigraphy of the Southern Ocean. In: Hayes D.E., Frakes L.A., et al. (eds.), *Initial Reports of the Deep Sea Drilling Project,* Washington, DC, US Govt. Printing Office, **28**, 515–570.

OggJ.G. & Smith A.G., 2004. The Geomagnetic Polarity Time Scale. In: Gradstein F.M., Ogg J.G. & Smith A.G. (eds.), *A Geological Time Scale*, Cambridge University Press, Cambridge UK, 63–95.

Ramsey A.T.S. & Baldauf J.G.,1999. A Reassessment of the Southern Ocean Biochronology. *Geol. Soc. London Mem.*, **18**, 1–122.

Renne P.R., Ownes T.L., DePaolo D.J., Swisher C.C., Deino A.L. & Karner D.B., 1998. Intercalibration of Standards. Absolute Ages and Uncertainties in $^{40}Ar^{39}Ar$ dating, *Chemical Geology*. **145**, 117–152.

Scherer R., Hannah M., Maffioli P., Persico D., Sjunneskog C., Strong C.P., Taviani M., Winter D. & the ANDRILL-MIS Science Team, this volume.Palaeontological Characterisation and Analysis of the AND-1B Core. ANDRILL McMurdo Ice Shelf Project. Antarctica. *Terra Antartica*.

Shaw A.B., 1964. *Time in Stratigraphy*. New York. McGraw Hill. 365 p.

Shipboard Scientific Party, 2001. Explanatory Notes. In: O'Brien P.E., Cooper A.K., Richeter C., et al. (eds.). *Proceedings of the Ocean Drilling Program. Initial reports.* College Station. TX (Ocean Drilling Program), **188**, 1-191 (online: http://www-odp.tamu.edu/publications).

Steiger R.H. & Jäger E., 1977. Subcommission on Geochronology: Convention on the Use of Decay Constants in Geo- and Cosmochronology. *Earth and Planet. Sci. Lett.*, **36**, 359–362.

Taylor J.R., 1982. *An Introduction to Error Analysis.* University Science Books. Mill Valley. CA.

Weaver F.M. & Gombos A.M., 1981. Southern High-Latitude Diatom Biostratigraphy. In: Warme T.E., Douglas R.G. & Winterer E.L. (eds.). *The Deep Sea Drilling Project: A Decade of Progress*. Special Publications of the Society of Economic Paleontology and Mineralogy, **32**, 445–470.

Whitehead J.M. & Bohaty S.M.. 2003. Pliocene Summer Sea Surface Temperature Reconstruction Using Silicoflagellates from Southern Ocean ODP Site 1165. *Paleoceanography*. **18**. 20–31.

Whitehead J.M. & Bohaty S.M., 2004. Data Report: Quaternary–Pliocene Diatom Biostratigraphy of ODP Sites 1165 and 1166. Cooperation Sea and Prydz Bay. In: Cooper A.K., O'Brien P.E.& Richter C. (eds.), *Proceedings of the Ocean Drilling Program, Scientific Results*. College Station, TX (Ocean Drilling Program). **188** (online: http://www-odp.tamu.edu/publications).

Winter D.M., 1995. *Upper Neogene Diatom Biostratigraphy from Coastal Drillcores in Southern Victoria Land, Antarctica*. M.S. thesis. University of Nebraska-Lincoln, Lincoln, Nebraska, 146 p.

Winter D.M. & Harwood D.M., 1997. Integrated Diatom Biostratigraphy of Late Neogene Drillholes in Southern Victoria Land and Correlation to Southern Ocean Records. In: Ricci C.A. (ed.), *The Antarctic Region: Geological Evolution and Processes, Terra Antartica Publication*, 985–992.

Winter D.M. & Iwai M., 2002. Data Report: Neogene Diatom Biostratigraphy. Antarctic Peninsula Pacific Margin. ODP Leg 178 Rise Sites. In: Barker P.F., Camerlenghi A., Acton G.D. & Ramsay A.T.S. (eds.), *Proceedings of the Ocean Drilling Program. Scientific Results,* College Station, TX (Ocean Drilling Program), **178** (online: http://www-odp.tamu.edu/publications).

York D.. 1969. Least Squares Fitting of a Straight Line with Correlated Errors. *Earth and Planet. Sci. Lett..* **5**. 320.

Zielinski U. & Gersonde R., 2002. Plio-Pleistocene Diatom Biostratigraphy from ODP Leg 177, Atlantic sector of the Southern Ocean. *Marine Micropaleontology,* **45**, 225–268.